Three-dimensional virtual retinal display using a deformable membrane mirror

Sarah C. McQuaide

A thesis submitted in partial fulfillment of the requirements for the degree of

Master of Science in Mechanical Engineering

University of Washington
2002

Program Authorized to Offer Degree: The Department of Mechanical Engineering

Table of Contents

		Page
List of Figures		iii
List of Tables		v
Chapter 1:	Introduction to the Thesis	1
Chapter 2:	Display Systems	2
	2.1 Introduction	2
	2.2 Human visual depth cues	2
	2.3 Types of 3D display systems	3
	2.3.1 Stereoscopic displays	4
	2.3.2 Volumetric displays	6
	2.3.3 Optical beam-modulating displays	8
	2.3.4 A new light-modulating display	9
Chapter 3:	The Virtual Retinal Display	10
	3.1 Introduction	10
	3.2 Components of the Virtual Retinal Display	10
	3.3 Advantages of the Virtual Retinal Display	11
Chapter 4:	MEMS	13
	4.1 Introduction	13
	4.2 How are MEMS made?	14
	4.3 What can MEMS do?	16
	4.3.1 Transportation	16
	4.3.2 Medicine	16
	4.3.3 Telecommunications	17
	4.3.4 Display systems	17
	4.4 The Future	18
Chapter 5:	Deformable Membrane Mirrors	19
	5.1 Introduction	19
	5.2 History	19
	5.3 MEMS deformable membrane mirrors	21
	5.4 DMM fabrication and research	21
Chapter 6:	Three-dimensional virtual retinal display system using a deformable membrane mirror	24
	6.1 Background	24

	6.2 Approach	26
Chapter 7:	Optical Design for the Monocular Display	28
	7.1 Optical train components	28
	7.2 Deformable mirror characteristics	31
	7.3 High-voltage amplifier for driving deformable membrane mirror	33
	7.3.1 Static operation of mirror	34
	7.3.2 Dynamic operation of mirror	34
Chapter 8:	Static testing of deformable mirror	35
	8.1 Mirror optical power outside of setup	35
	8.2 Mirror optical power within the setup	36
	8.2.1 Measurements with beam profiler	36
	8.2.2 Human subject experiments	38
	8.3 Visual changes in the display at various focal planes	40
Chapter 9:	Dynamic testing of deformable mirror in ambient air pressure and high vacuum	41
Chapter 10:	Modeling the deformable membrane mirror	44
	10.1 Finite element model	44
	10.2 Calculation of electrostatic force and membrane tension	45
	10.3 Theoretical frequency response	50
	10.4 Comparison of experimental results with theory	52
Chapter 11:	Discussion and future work	55
	11.1 Expansion to bi-ocular display	55
	11.2 Challenges	57
	11.3 Use of a deformable mirror in a non-scanning display	59
Chapter 12:	Conclusion	61
References		62
Appendices		
	Appendix A: Deformable membrane mirror instructions as supplied by OKO Tech	66
	Appendix B: Voltages for static and dynamic driving of deformable mirror	67
	Appendix C: Operation of the Deformable Membrane Mirror Driver	68

List of Figures

Figure Number		Page
2.1	Perception of a stereoscopic image	4
2.2	A lenslet light-modulating display	6
2.3	Examples of volumetric display systems	7
2.4	Light wavefronts entering the eye	8
3.1	Schematic of the light raster scan onto the retina	11
3.2	Illustration of light raster scan onto the retina	11
4.1	MEMS markets and expected growth rates by 2001	14
4.2	Basic surface micromachining process	15
4.3	MEMS device examples	18
5.1	Example of a deformable membrane mirror architecture	21
6.1	Accommodation-vergence mismatch	24
7.1	Diagram of optical setup	28
7.2	Photo of monocular optical setup	28
7.3	Schematic of single beam traces	29
7.4	Three positions of the scanning beam focused on retina	30
7.5	Subject viewing image through scanned display	30
7.6	Image at optical infinity with no voltage on mirror	31
7.7	Image at optical infinity with maximum voltage on mirror	31
7.8.	Schematic of OKO deformable membrane mirror	32

7.9	Front view photograph of mirror	32
7.10	Schematic of mirror driver	33
8.1	Diagram of optical setup (repeated from Figure 7.1)	36
8.2	Applied voltage on mirror and corresponding optical power	38
8.3	Average spherical equivalent of 10 subjects' accommodation to variable-focus VRD	40
9.1	Deformable mirror being tested under high vacuum	41
9.2	Frequency response curve of deformable mirror	42
10.1	FEA model of deformable mirror at 300 V applied voltage	45
10.2	Diagram showing values used in membrane deflection calculation	46
10.3	Applied voltage on mirror versus membrane tension	49
10.4	Applied voltage on mirror and corresponding theoretical first resonant frequency in vacuum	51
10.5	Frequency response curve of deformable mirror (repeated for reference from Figure 9.2)	52
10.6	Schematic of deformable mirror dynamic structural response	53
11.1	Photograph of bi-ocular retinal light scanning display	56
11.2	Schematic of bi-ocular retinal light scanning display	56
11.3	DMM manufactured by Intellite, Inc.	57
11.4	Example of a display configuration with blocked planes of depth	59
11.5	Design for an LCD display screen utilizing a deformable mirror	60

List of Tables

Table Number		Page
2.1	Classification of 3D display systems	4
7.1	Lens focal lengths and locations within the optical setup	28
7.2	DMM specifications as supplied by manufacturer OKO Tech	32
8.1	Mirror raw optical power	35
8.2	Focal point of light striking the deformable mirror within optical setup	37
8.3	Accommodation data taken from 10 human subjects	39
10.1	Known values used in calculation of membrane tension	48
10.2	Values used in calculation of theoretical first resonant frequency in vacuum	51
11.1	Monocular display characteristics	55

Acknowledgements

I wish to express great appreciation to my advisor, Professor Eric Seibel, PhD, for his support throughout the course of my master's study. Also greatly appreciated are the efforts of Robert Burstein, my continual friend, artist, and tinkerer, with an endless capacity for making things work. Thanks is extended to Professor Per Reinhall for his help in the vibrations and modeling portions of this thesis. My friends at HIT lab are to be acknowledged as well, for their smiles and laughter every day throughout the course of my work there.

We also acknowledge financial support from a gift by the Intel Corporation.

Chapter 1: Introduction to the thesis

A deformable membrane mirror is being used to generate multiple focal planes within a scanned light display, or virtual retinal display (VRD). The MEMS deformable mirror changes the focal plane of the display by varying the wavefront of the optical beam entering the eye. Dynamically changing the focal plane will allow the viewer to see 3-D objects using the natural accommodative response of the eye, unlike current stereographics that rely on retinal disparity. The display system can successfully generate a focal range from zero to 3 diopters, verified through laboratory beam profiling data and human subject experiments. Future work will involve expanding the system to a bi-ocular and, eventually, binocular system that will provide separate images to both eyes, meeting the final goal of a full-color, variable focus stereographic display.

Chapter 2: Display Systems

2.1 Introduction

In daily life, human beings are surrounded by a three-dimensional world. We see, feel, and interact with objects that have depth and dimension. The human visual system has thus naturally evolved to understand information displayed in three dimensions. A great limitation of two-dimensional displays is that they cannot convey the kind of information most easily processed by the human visual system. Whether it is in medicine, flight simulation, computer-aided design, or entertainment, the advantages of utilizing three dimensions over two are immense. There has been great advancement in the development and rendering of three-dimensional images, as well as the memory capacity to contain the data that describe them. The actual *display* of these images, however, has not developed at such a rapid pace and has become a significant engineering challenge.

2.2 Human visual depth cues

Before a more detailed description of 3D displays, it is useful to understand how the human visual system works. In order to effectively portray three dimensions, a display must satisfy certain depth cues in the visual system. These cues range in strength in terms of the degree of depth sensation they invoke, and are grouped into the following categories: (1) binocular disparity, (2) motion parallax, (3) vergence, (4) accommodation, and (5) pictorial cues (Sugihara and Miyasato, 1998). *Binocular disparity* is the difference in perspective that each eye sees as a result of its position relative to an object. The left and right eyes see slightly different views, and when these views are processed in the brain they invoke the perception of depth. *Motion parallax* is the sense of depth one perceives from a moving image, in which close objects move farther across the field of view than distant objects. *Vergence* is the movement of the eyes inward or outward to fixate on a target, while *accommodation* is the change in shape of the crystalline lens of the eye to bring a target into focus. Finally, *pictorial cues* are cues such as perspective,

occlusion, blur, etc. which are dependent on the rendering of an image and are usually the responsibility of the image source, not the display system itself.

The cues of accommodation and vergence together pose a challenge in 3D displays. An emmetropic (normal) eye will view objects clearly at various focal distances by both accommodating and verging to a target. These two perceptual processes are linked at a muscular level: a change in accommodation triggers a change in vergence, and vice versa (Rinalducci et al., 1983). When an object's perceived position in space is different from the position from which it is displayed, the eyes must accommodate to one distance while verging to another. In display systems that force the visual system to uncouple accommodation and vergence, problems such as eye strain, fatigue, and/or loss of visual acuity can result (Mon-Williams et al., 1993). This problem is discussed in more detail in section 6.1.

2.3 Types of 3D display systems

Most 3D display systems fall into one of three categories depending on the mechanism of 3D representation: stereoscopic, volumetric, or optical beam-modulating (Sugihara and Miyasato, 1998). See Table 2.1. The first type, stereoscopic, will be defined for the purposes of this paper as a display generating only a binocular disparate image supplied to each eye separately. The second two types, volumetric and optical beam-modulating, can represent a 3D image spatially and may satisfy the depth cues of motion parallax, vergence, and accommodation. Each display category has been produced commercially, and each has its own strengths and weaknesses.

Table 2.1. Classification of 3D display systems

	Stereoscopic	**Autostereoscopic**	
		Volumetric	Optical beam modulating
Types of devices	HMD Shutter glasses Lenticular screen Polarized filter	Varifocal mirror Moving LED panel Mechanical rotating screen Multiplanar optical elements	Holography Luminance-modulating Depth-modulating
Remarks	binocular disparate image supplied to each eye; may require glasses or other viewing aid	Represent 3D image spatially and can satisfy depth cues of motion parallax, vergence, and accommodation	

2.3.1 Stereoscopic displays

Stereoscopic displays are one of the most common 3D display systems used today, in which a sense of depth is generated by providing two separate views, one to each eye. See Figure 2.1. Since binocular disparity is known to be a strong depth cue even in the absence of other cues (Julesz, 1960), stereoscopic displays are effective for many practical applications. Stereoscopic images can be implemented with a simple device configuration and low data rates, requiring only the presentation of two perspective views.

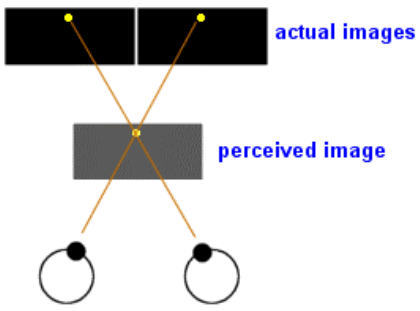
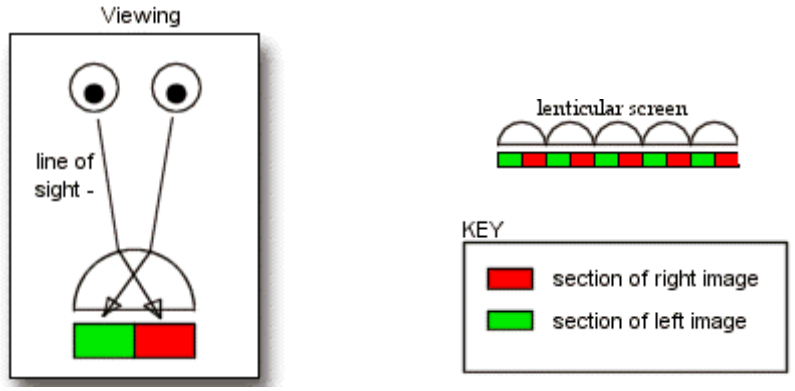


Figure 2.1. Perception of a stereoscopic image. Stereoscopic displays provide two slightly different views to each eye.

Images can be displayed stereoptically in a number of ways. Some require the use of shutter glasses, as in the case of 3D Imax films. The shutter glasses are in sync with the screen, alternately displaying two images with some degree of disparity to the eyes that are then fused by the visual system. Other stereoscopic displays are head-mounted, with an individual screen for each eye displaying slightly different perspective views of an image. Some of these are consumer-marketed, such as I-O Display System's i-Glasses (I-O Display Systems, 2001). The i-Glasses have an 800x600 liquid-crystal display with a 26-degree diagonal field of view, for about $1600. Professional industrial stereo displays are also available with greater resolution and fields of view, such as the SimEye XL100A made by Kaiser Electro-Optics, Inc. for $87,500 (Kaiser Electro-Optics, Inc., 2001). The display has a resolution of 1024x768 and a field of view of 50˚ vertical by 100˚ horizontal.

In another form of stereoscopic displays, an array of lenses called a "lenslet" is used (Halle, 1997). See Figure 2.2. A lenslet is set over an LCD or other image source, each lens having the same dimensions as the pixels it covers. The light emerging from the image source is set one focal length behind the array of lenses so that it emerges collimated from the lens. The optical power of the lens determines the angle through which the image can be seen by a viewer.

Stereographics Corporation (Stereographics Corp., 2000) manufactures an LCD monitor with semispherical lenslets lying in a plane, which direct perspective views of an image into a central cone-shaped viewing zone. More viewing zones to the right and left of the main zone let additional people view the stereo image.



http://www.nvnews.net/articles/3dimagery/natural.shtml

Figure 2.2. A lenslet light-modulating display. A lenslet is a simple array of lenses set over an image, displaying a slightly different viewing angle to each eye.

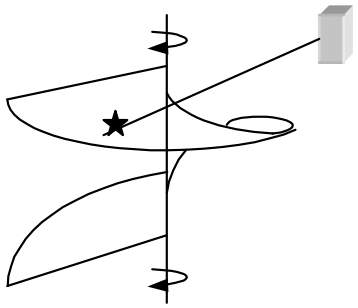
Although stereoscopic images have the advantage of being opaque, making pictorial depth cues such as occlusion and motion parallax possible, they allow for only one perspective view of a scene; a viewer cannot "walk around" a scene and view it from different angles. In addition, stereographic displays do not allow for accommodation-vergence synkinesis, requiring viewers to uncouple these two natural visual responses.

2.3.2 Volumetric displays

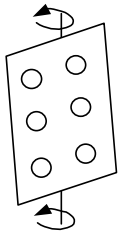
Volumetric displays are devices capable of depicting images within a physical volume. See Figure 2.3. One of the first ways this was done was to project an image onto a mirror membrane, which deformed via air pressure changes produced by a loudspeaker (Mills et al., 1984). The mirror displayed 3D objects by sequentially presenting z-slices of the image so that the projected image depth corresponded to the actual depth of that slice of the object. When presented at a fast enough rate (about 15kHz), the visual system would provide the fusion required to see a 3D image. Other volumetric displays have used two-dimensional arrays of light emitting through a 3D volume (Travis, 1997), or projected image slices onto multiplanar optical elements (Depthcube, Inc., 2001). An innovative recent approach by Suyama, et al. used a dual-frequency liquid-crystal varifocal lens

synchronized with a 2-D display to provide a 3D image (Suyama, Date, et al., 2000). The molecules within the liquid-crystal lens change their orientation in response to a change in amplitude of the applied electric field, creating a range of lens shapes from concave to convex. A focal-length range of –1.2 to + 1.5 diopters (1/m) was accomplished.

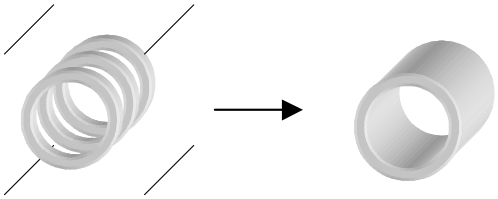
Because they create an image within a physical volume, holographic displays are also sometimes classified as volumetric displays. Here, however, they will be classified as light-modulating displays as they create an image by reconstructing divergence information from light emitted by an object.



(a) Light is projected onto a rotating translucent screen, creating a 3D volume.



(b) A 2D array of spinning LEDs creating a 3D volume.



(c) The Depthcube volumetric display projects slices of an image onto planar optical elements to create the sensation of depth.

Figure 2.3. Examples of volumetric display systems.

2.3.3 Optical beam-modulating displays

Optical beam-modulating displays encompass systems in which a beam's wavefront and/or intensity is varied. With a change in wavefront, the amount of divergence of light entering the eye is changed, a technique called "wavefront shaping" for the purposes of this thesis. Objects at optical infinity have flat wavefronts, while objects closer than infinity have some degree of curvature based of their distance from the retina See Figure 2.4. The human visual system perceives depth when the eye's crystalline lens changes shape in order to focus these incoming beams.

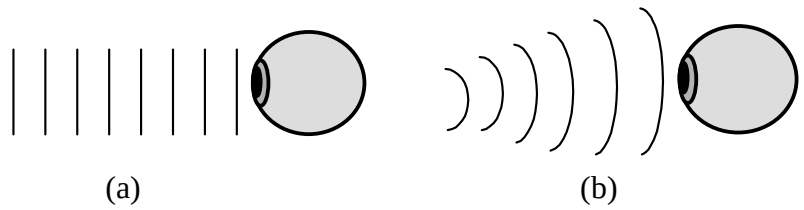


Figure 2.4. Light wavefronts entering the eye from (a) an object located at optical infinity and (b) an object closer than optical infinity.

One example of a display using wavefront shaping is the hologram. Wavefront information about an object is stored as interference fringes during an exposure process and is then reconstructed as an image of the object when illuminated (Halle, 1997). Standard liquid-crystal displays can be used to display a hologram; however, wide fields of view are not possible because of the substantial amount of pixellation required. Acoustooptic modulators can also be used to display holograms, but again the problem of limited fields of view is arises due to the high phase modulation rate (Travis, 1997). In spite of these challenges, the recent technique of electro-holography, the process of forming a fringe pattern electrically, has made holograms effective for certain applications. Voxel, Inc. is manufacturing a Digital Holography System (Voxel, Inc., 2001) for commercial use that works with existing medical imaging equipment to produce images of tissues, organs, etc. to help doctors visualize anatomical data.

In an intensity-modulated display, the luminance of optical light beams is varied. NTT Cyber Space Laboratories (Suyama, Takada, et al., 2001) have developed an intensity-modulated display called the Depth-Fused 3-D Display (DFD) in which two 2D images are displayed at different depths to enable viewers to perceive a 3D image. Two LCD screens are used in combination with a beamsplitter to create an image lying within a focal range from forward of the first screen to beyond the second. The authors show that the image appears outside of the region of the two display images when there are opposite signs of luminance between an object and its surroundings. The image appears between the two display images when the luminance between the screens is divided at some ratio.

2.3.4 A new light-modulating display

It is the display of images using wavefront shaping, and ultimately a combination of wavefront shaping and intensity modulation, that is the interest of this thesis. While previous 3D displays have not allowed for accommodation-vergence synkinesis, this thesis describes a 3D light-modulating display system that uses a novel technique to allow viewers to accommodate and verge to the same plane in space as in natural viewing. The system has the potential to become a head-mounted display as well as provide both opaque and transparent images. These advantages along with others will be discussed in the following chapters.

Chapter 3: The Virtual Retinal Display

3.1 Introduction

The Virtual Retinal Display (VRD) was invented in 1993 at the University of Washington Human Interface Technology (HIT) Lab (Furness and Kollin, 1995). The VRD uses modulated low-power laser light to generate a scanned image directly to the retina, essentially "painting" a picture onto the eye. A small beam of light is focused onto the retina and is swept over it in a raster pattern. In this way, a full-color image with a wide field-of-view, high resolution, and high brightness is produced. The VRD has the versatility to provide an augmented view (in which the scanned scene is overlaid onto the real world as a transparent image) or an occluded view (in which the display provides fully inclusive opaque images).

3.2 Components of the Virtual Retinal Display

The VRD uses a coherent light source such as a laser which is modulated to display light of a certain intensity to form the image being rendered. See Figures 3.1 and 3.2. The beam is raster-scanned using standard video sources to direct each pixel to its proper place on the retina. In the original configuration of the VRD, a mechanical resonant scanner is used for the fast horizontal scan while a galvanometer produces the slower vertical scan. An input video signal is fed to drive electronics, which synchronize the VRD scanners with the intensity modulators to form an image. The raster scan is directed through final viewing optics, which serve to both collimate the scanned rays and converge the scan into a viewing exit pupil. When the viewer aligns his eye at the exit pupil, a virtual image appears in the distance. The VRD can produce 640 x 480 resolution at 60 Hz frame rates. Subsequent versions of the VRD have included an interactive VRD with integrated head tracking and a head-mounted monochrome version.

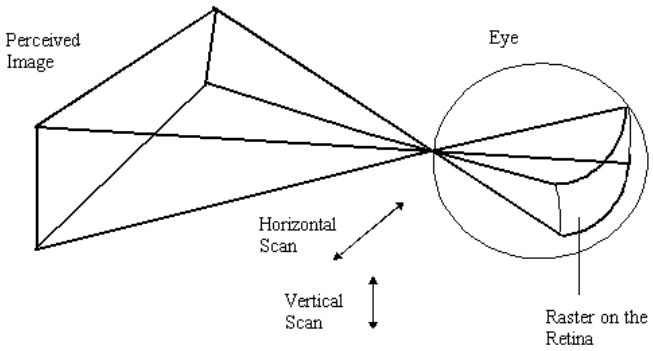


Figure 3.1. Schematic of the light raster scan imaged onto the retina and the resultant perceived image. Courtesy Mike Tidwell, University of Washington.

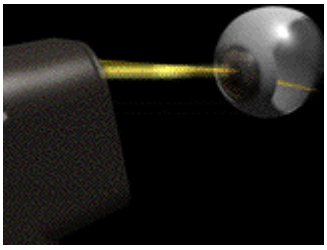


Figure 3.2. Illustration of light raster scan onto the retina.
Courtesy Quinn Smithwick,
University of Washington.

3.3 Advantages of the Virtual Retinal Display

The VRD has many advantages over conventional displays using LCD's or CRT's. Since the only light losses in the VRD are due to optics, the VRD is much brighter than conventional displays using individual pixel emitters (Tidwell, 1995). With individual liquid crystal cells or phosphors, a decrease in pixel size increases display resolution but decreases luminance since the smaller pixels emit less light. In the VRD, beam intensity and resolution are independent, creating a very bright display that is easily seen in an augmented mode in which the outside environment and the virtual environment are seen simultaneously. The VRD also has the advantage of being dependent only on a light source and functional scanners, whereas a conventional display depends upon the reliability of individual pixels. Finally, the theoretical size for horizontal and vertical scanners including light sources for the VRD is smaller than the size of conventional liquid crystal array and CRT image sources. The further introduction of smaller light sources such as laser diodes and smaller mechanical scanners show great promise for a small, lightweight head-mounted display.

As will be explained in detail in the following chapters, the VRD is being modified from a fixed plane of focus display to a variable-focus display with the potential to become an immersive, high-resolution 3D display.

Chapter 4: MEMS

4.1 Introduction

Though the everyday person or even the scientist may not be aware of it, a phenomenal technology has been developing for the past decade. MEMS, or microelectromechanical systems, are on the verge of making the same kind of impact on the world market that integrated circuits did. Shipments of MEMS worldwide in 2000 equaled $14.2 billion and are forecast to grow to $30.4 billion (Pfeiffer, 2001) in the coming four years. See Figure 4.1 (Grace, 2000). The MEMS market is mirroring the way the semiconductor market began in the late 1960s: there are no overall leaders in the MEMS industry, just a number of smaller companies working to perfect and advance current technology. So what exactly are these tiny devices that will play a key part in machines of the future?

Microelectromechanical systems, as the name first implies, are very small, contain electronic and mechanical parts, and are systems whose parts are integrated to perform together in some sort of package. The earliest MEMS devices were pressure sensors, developed by Honeywell in 1962 after C.S. Smith discovered that silicon could sense pressure better than metal (Pfeiffer, 2001). Later devices included accelerometers used to actuate car airbags, microvalves and pumps used in medicine, switches used in optical communications networks, and micromirrors used in data transmission. In the early 1990s Saab became the first company to do what all MEMS designers are trying to achieve now: integrate both the MEMS device and its accompanying circuitry on the same chip, making fabrication of the entire device possible in any IC-circuit facility (Pfeiffer, 2001). In fact, most MEMS processes are borrowed from the IC industry and their fabrication follows many processes found in CMOS, the integrated-circuit process (Boehringer, 2002).

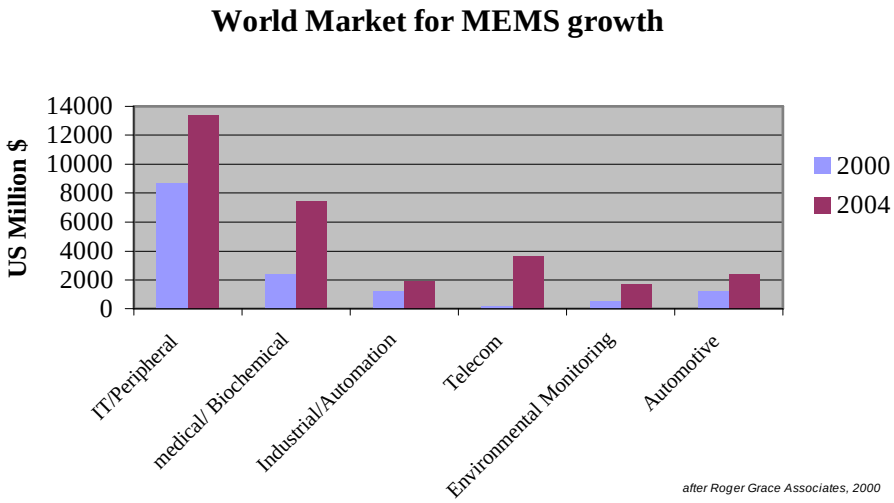


Figure 4.1. MEMS markets and expected growth rates by 2004.

4.2 How are MEMS made?

Following processes borrowed from integrated-circuit chip production, MEMS fabrication is based on lithographic techniques. A substrate wafer is used as a base material upon which other materials are added and/or removed using photosensitive materials, light exposure, and various etchants. A large number of devices can be fabricated on one chip, decreasing production costs when manufacturing is done in high volume. The most commonly used substrate material is silicon, for a number of reasons- it is the most common material used in IC production; it is available in virtually pure form; its material properties are very well known; it is a semiconductor; and it is very strong and light (Senturia, 2000).

There are two major fabrication techniques in MEMS production: bulk micromachining and surface micromachining. In bulk micromachining, the Si wafer and any added insulating layers provide the entire structural material for the device. In surface micromachining, thin films of other materials are deposited on the surface of the wafer, forming the structural material. See Figure 4.2. These layers are then patterned and

etched a number of times, allowing for great flexibility in the ultimate design of a structure.

The additive materials used in surface micromachining are chosen to provide conducting and insulating layers. These materials include silicon in various forms (amorphous, polycrystalline, epitaxial), silicon compounds (oxides, nitrides, carbides), metals and metal compounds, glass, ceramics, polymers, and other inorganics (Kovacs, 1998).

The removal of material during etching can take place in one of two ways: isotropically or anisotropically. During isotropic etching, chemicals are used that etch the material at the same rate in all directions, resulting in a rounded corners and sometimes spherical-shaped voids. During anisotropic etching, a chemical is used which etches the material along its crystal planes, resulting (if one uses chemicals with good selectivity of one crystal plane over another) in near-perfect flat surfaces. The method used depends on the desired characteristics of the device.

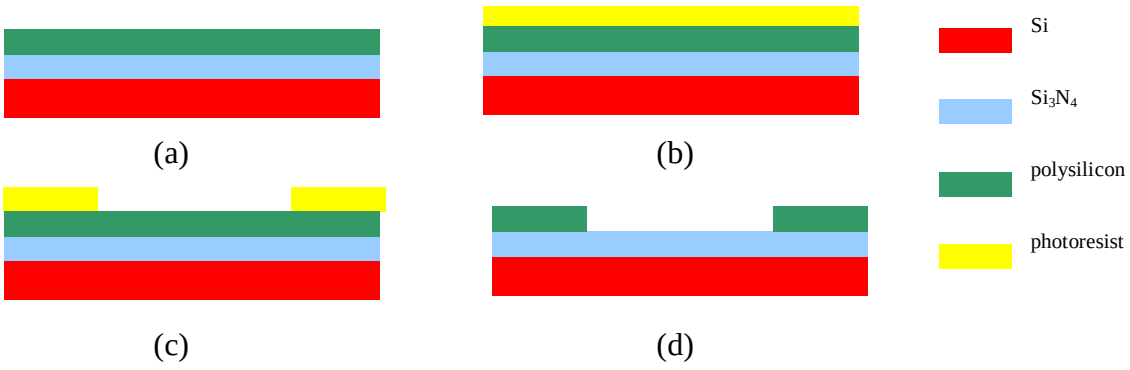


Figure 4.2. Basic surface micromachining process. In (a), a protective isolation layer of Si_3N_4 and a structural layer of polysilicon are deposited on the bulk Si wafer. A layer of photoresist is added (b) and patterned (c) using photolithography. During etching, the parts of the Si_3N_4 layer not covered with photoresist (if using a positive-type mask) are etched away, leaving a patterned structural layer.

4.3 What can MEMS do?

Although the market for MEMS began in a very small niche, pressure sensors, it is now expanding into many other areas.

4.3.1 Transportation

As a result of the many microdevices used in automobiles today, the automotive industry has been one of the main forces behind the development of MEMS. Accelerometers are one of the most important MEMS devices utilized in cars, protecting the safety of passengers by deploying airbags when sensing movement of a small mass within the device previous to an impact. Pressure sensors are another MEMS device used in quantity in automobiles, monitoring engine and tire pressure. MEMS are even used in some car alarm systems to sense a change in the position of the car. The BMW 740i epitomizes the MEMS-stacked vehicle with over 70 MEMS sensors (Pfeiffer, 2001). The aerospace industry is another key consumer of MEMS devices for use in jet engines as pressure and chemical sensors.

4.3.2 Medicine

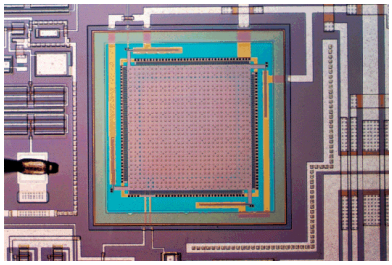
“BioMEMS” are utilizing the micro-proportions of MEMS devices to solve problems in the human body that previously would have been impossible. BioMEMS research is currently being done in drug delivery (Langer, 2002), blood pressure monitoring, and diagnostic “lab on a chip” devices (Pfeiffer, 2001). Many institutions including the University of Washington are conducting research in microprobes: devices that will allow investigation of nervous tissue by way of self-implantation on the interior of nervous cells (Denton, et al., 1999). The research hopes to lead to a better understanding of the workings of the nervous system and allow for communication with nervous tissue. The University of Ann Arbor, Michigan, is developing a cochlear implant that uses microelectrode arrays to bypass damaged cilia within the auditory nerve, helping deaf people hear again (Wise, 2001).

4.3.3 Telecommunications

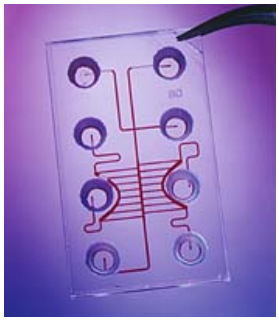
The prevalent use of cell phones and the internet today has caused the need for optical networks to rise drastically. MEMS are providing the optical devices needed for fast switching of light to a certain optical fiber and path. Many companies are involved with optical MEMS development, including Lucent, Nortel Networks, Corning, and JDS Uniphase (Pfeiffer, 2001). In another telecommunications application, MEMS are being used in cell phones to miniaturize bulky components such as band-pass filters, making phones the size of a wristwatch feasible (Discera, 2001).

4.3.4 Display systems

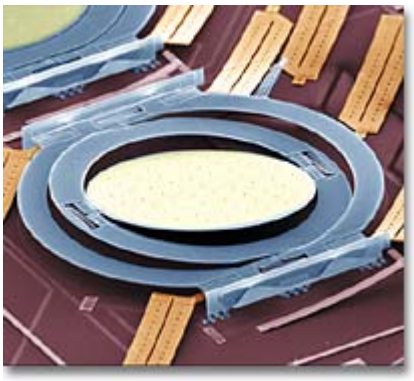
Texas Instruments has developed a technology using MEMS micromirrors that tilt to modulate light intensity (Texas Instruments, 2002). Large projection displays of this type have incredible clarity because they output a digital image and bypass the need that current displays have of translating a digital input to an analog output. Microvision Inc., a company launched from the University of Washington Human Interface Technology Lab, is using MEMS bi-axial mirrors in high-frequency scanners for their retinal scanning display systems (Microvision, 2002). The head-mounted retinal displays utilize MEMS scanners over the former technology, which used galvanometers and mechanical resonant scanners to produce the horizontal and vertical scan. This thesis describes a MEMS deformable membrane mirror used to modulate the wavefront of light entering the eye.



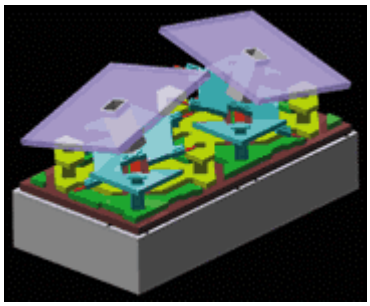
(a)



(b)



(c)



(d)

Figure 4.3: MEMS device examples.
(a) Accelerometer, (imi-MEMS, 2001). (b) diagnostic lab-on-a-chip, (Agilent Tech., 2001). (c) optical switch, (Lucent Tech., 2000). (d) micromirror, produced by Texas Instruments (Texas Instruments, 1997).

4.4 The Future

There is no doubt that MEMS are going to play a large role in the devices of the future. Aside from industrial applications, common consumer devices will soon contain MEMS, improving device function and downscaling size. Consumer electronics should be one of the biggest markets, using MEMS for data storage in digital camera memory chips and wristwatch phones (Pfeiffer, 2001). The gaming industry is expected to use MEMS in joysticks and motion-sensing devices. MEMS could be used in washing machines as balance sensors, and in microwaves to adjust power levels for different altitudes. Since the applications are so vast and the market is not dominated by one key player, a number of companies should benefit from the impact MEMS will make on technology.

Chapter 5: Deformable Membrane Mirrors

5.1 Introduction

The deformable membrane mirror (DMM) is a device used in adaptive optics applications. In general, the architecture of DMMs consists of a thin membrane set over one or more electrodes which actuate the mirror and cause it to deform locally in a parabolic shape. When light shines on the mirror surface at a constant angle of incidence, the wavefront of the output beam of light is changed according to the mirror surface. In this way an aberrated beam of light can be corrected, or an input beam can be altered to produce a desired output wavefront shape.

5.2 History

Early DMMs were large-scale (>10 cm, Grosso and Yellin, 1977) with multiple electrodes, and were used in telescopes to focus incoming aberrated light from space to form a clearer image. Later, DMMs began to be produced as MEMS devices for increased versatility and lower cost.

When a simple lens is used to create an image, the parts of the image located off-center of the lens field of view are not optimally formed. The aberrations caused by this phenomenon can be corrected using optics that compensate for the difference in imaging requirements throughout the field of view. This can be accomplished using custom lenses that have variable surfaces, but the manufacture of these lenses is time-consuming and expensive (Dickensheets, Ashcraft, et al., 1999). A DMM can accomplish the same task with a simpler, cheaper approach: a continuous membrane changes shape in response to an actuator, creating a surface that matches the required shape.

One of the first DMMs was developed by Itek Optical Systems in 1973 and was controlled by 349 piezoelectric actuators (Ealey, 1991). The mirror itself was an 0.05 inch glass sheet and required 3000 V of potential to drive the lead zirconate titante (PZT)

electrodes. An improved version developed in 1979 using lead magnesium niobate actuators had improved performance and lowered voltage requirements. However, the actuator voltage was still in the kV range and lower drive voltages were required by much of the adaptive optics community.

An improvement came in the late 1970s with the development of electrostatically-actuated deformable membrane mirrors by Grosso and Yellin at the Perkin-Elmer Corporation (1977). The mirrors were used by NASA for wavefront correction of images from ground telescopes as well as for solar power collection. Made of titanium sputtered onto a CaF_2 substrate, the mirror was tensioned into a ring and epoxied into place. It was then encapsulated in a chamber with a window and operated at a low vacuum pressure of 2 Torr to decrease membrane damping and increase operational bandwidth. An array of electrodes on the backside of the mirror applied a voltage that changed the degree of membrane deflection in its local area.

Subsequent large-scale membrane mirrors were similar in operation, while the materials used to make them improved in surface quality. In the late 1980's companies including Hughes, Rockwell, and Lockheed investigated the use of cooled DMMs for correction of aberrations caused by high-energy laser light progression through the atmosphere (Ealey, 1991). Johns Hopkins University developed a membrane mirror made of cellulose and stretched over 90 actuators (Martin et al., 1997). The mirror was used in a device called a coronograph, which blocks the bright inner disk of the sun so that the corona can be studied.

5.3 MEMS deformable membrane mirrors

Many current deformable membrane mirrors are micromachined MEMS devices, making mass fabrication very simple and cost-effective since multiple mirrors are fabricated on a single wafer. The mirrors are also more useful in the increasing number of devices that require small or micro components. The applications today for DMMs are broad, encompassing telecommunications, optical data storage, laser machining, and adaptive optics for imaging and scanning (Intellite, 2002). Figure 5.1 shows an example of a general deformable membrane mirror architecture. The mirror is bulk micromachined, with the silicon wafer serving as the substrate. A silicon nitride layer coated with a reflective layer of aluminum forms the moveable membrane. A printed circuit board with an electrode is epoxied to the backside of the wafer for electrostatic actuation.

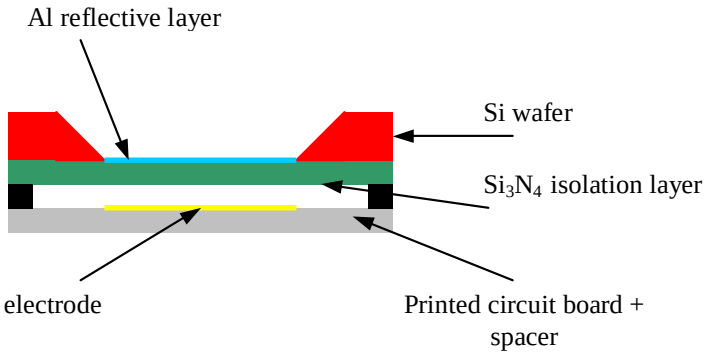


Figure 5.1. Example of a deformable membrane mirror architecture.

5.4 DMM fabrication and research

There are a number of key players emerging in DMM fabrication who are producing most of the mirrors used in current research. Cronos, a division of JDS Uniphase, has developed a commercial program called Multi-User MEMS Processes (MUMPS) that allows a user to design a MEMS device and have it prototyped and fabricated at the Cronos facility (Cronos, 2000). The MUMPS process allows for any kind of MEMS device to be fabricated within the bounds of certain guidelines that allow Cronos equipment to produce the desired design. An optical MEMS fabrication group at

Montana State University (Dickensheets, 2000) is using the MUMPS process to fabricate deformable membrane mirrors for use in planetary exploration in a project headed by NASA. The mirrors provide focus control for scanning image acquisition of rocks and soil on Mars.

Flexible Optical OKO is a manufacturer that specializes in MEMS deformable membrane mirrors (Oko-Tech., 2001). OKO fabricates DMMs for scientific and commercial use in atmospheric correction, ophthalmology, communications, holographic memory data storage, and optical fiber switching. The mirrors are fabricated from a silicon nitride membrane suspended over one or more electrodes and range in size from 5-50 mm in diameter. The smaller 5-mm mirrors have a single actuator and are used for simple defocus correction, while the largest, 50mm in diameter with 119 actuators, are used in space telescopes.

Another emerging company specializing in MEMS deformable membrane mirrors is Intellite, Inc. (Intellite, 2002). Intellite uses a novel mirror architecture that prevents a common membrane mirror problem called “snapdown” from occurring. When an electrode applies too much force to a membrane, the membrane can snap down to the electrode, sticking to it and breaking or damaging the mirror. Intellite’s design incorporates pillars which hang beneath the membrane and prevent it from sticking to the electrode should snapdown occur. The membranes have been tested in repeated trials and are fully recoverable from snapdown. Intellite’s customers use the mirrors in laser machining, photolithography, optical data storage, ophthalmologic medical imaging, and atmospheric devices.

A collaborative source of DMM and other optics research is lead by the Center for Adaptive Optics (CfAO), an organization funded by the NSF to promote collaboration in adaptive optics (http://cfao.ucolick.org). A number of CfAO members are doing research

in deformable mirrors, including industrial companies Xinetics, Inc. and Turn, Ltd. as well as the University of California at Berkeley and the University of Rochester.

Chapter 6: Three-dimensional virtual retinal display system using a deformable membrane mirror

6.1 Background

As discussed in section 2.2, three-dimensional display systems often cause a conflict within the human visual system by requiring viewers to accommodate to a fixed plane in space while changing their vergence angle. In the natural human visual system, accommodation and vergence are important physiological processes that are linked at a muscular level to allow the eye to view 3D objects: a change in accommodation can cause a change in vergence, and vice versa. Current electronic 3D displays cause conflict between these two perceptual processes, requiring viewers to uncouple their natural accommodation and vergence responses. A viewer must keep his accommodation fixed while his vergence is changing.

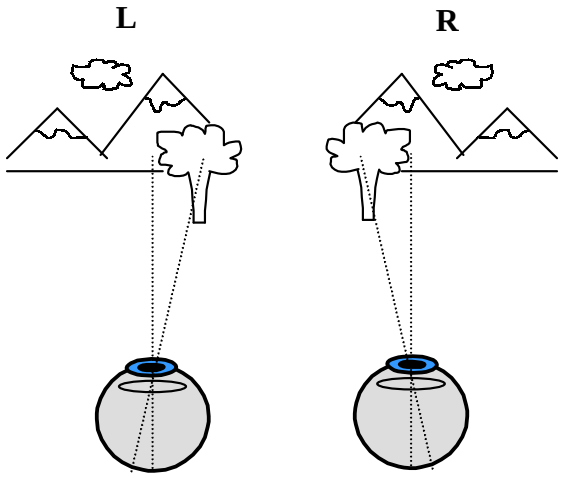


Figure 6.1. Accommodation-vergence mismatch. Current electronic 3D displays cause conflict between these two perceptual processes, requiring viewers to keep their accommodation fixed while vergence changes. To see clear images on a 3D display, the eye's crystalline lens must remain at a constant focal length as vergence changes whereas in normal viewing the focal length changes with vergence.

In certain people, the accommodation-vergence response is strongly linked, while in others it is not. In a study by Miyao et al. (Miyao, 1996), subjects performed a stereographic task where a target moved through a virtual gate. Subjects were asked to focus on the target and press a button when the object moved through the gate. Those who performed the task well, i.e., subjects who could easily decouple their accommodative-vergence response, complained of visual fatigue and exhibited loss of accommodation and decreased task performance. One subject with mild hyperopia (+2.0 D in both eyes) experienced extreme fatigue to the point of motion sickness. Another subject with mild phoria (unequal pull of one or more of the eye muscles) could not fuse the stereo images and did not complain of visual fatigue. The findings suggest that viewers who have strong accommodation-vergence synkinesis are able to view electronically-generated stereo images but experience fatigue and other visual problems, while those who have a weak accommodation-vergence response may not experience fatigue but also may not be able to fuse a stereo image in the first place.

Additional studies using head-mounted displays (HMDs) have suggested even stronger degrees of visual fatigue when accommodation and vergence distances are not matched. Mon-Williams (Mon-Williams et al., 1993) observed shifts in heterophobia in subjects viewing stereo HMD images. Heterophobia is a clinical measurement of visual stress, found by observing any changes in vergence angle when retinal disparity is removed with a lens that prevents binocular fusion. When a range of disparities is presented to the eyes to create different depth planes in a display, heterophobic shifts must take place within the viewer for each viewing distance. These shifts have been found to cause stress on the visual system. Mon-Williams suggests that a fundamental cause of this stress may be the conflict between the natural accommodation and vergence responses these displays cause. In addition, HMDs tend to have higher degrees of retinal disparity between the two stereo images presented to the eyes than non-head-mounted displays, further aggravating the problem (Wann, 1995).

Because of the significant differences in visual system responses among people, the ideal display system is one that can accommodate any perceptual conditions (Miyao, 1996). It is clear that a 3D display allowing for natural human visual responses including accommodation-vergence synkinesis would be superior to existing systems by providing both a more compelling experience of 3D viewing as well as reducing the possibility of visual fatigue.

There have not been many attempts to provide both accommodative and vergence depth cues in a 3D display system in the past because the integration of the two cues in a 3D display is a difficult technological challenge. In addition, because binocular disparity is considered a strong depth cue while accommodation is a weak depth cue (Boff and Lincoln, 1998), display makers have been able to create satisfactory 3D images without including both accommodation and vergence depth cues.

6.2 Approach

In order to investigate the effects of a display system incorporating accommodation and vergence depth cues, the Virtual Retinal Display (VRD) system at the University of Washington is being converted from a fixed-plane-of-focus display to a variable-focus display that allows for both accommodation and vergence to occur. The design of this "true 3D" display system is being accomplished in part by the use of a MEMS deformable membrane mirror that dynamically changes the wavefront of the light entering the eye, allowing each ray to be focused individually to different planes in space. The goal of the project is to create a variable plane of focus with a range of at least 0 to 3 diopters, or 0.33 m to infinity.

Two patents on the technology of retinal light scanning disclose methods for producing an accommodative cue for a true 3-D image display. The Sony Corporation owns a patent that includes methods using variable focus lenses, mirrors, liquid crystal and/or electro-optical lenses (Ashizaki et al., 1994). To the author's knowledge this technology has not

been pursued by Sony. The University of Washington owns a patent (Furness and Kollin, 1995) using the idea of dynamically varying the wavefront of light entering the eye using a deformable membrane mirror, the technology described in this thesis.

The following chapters of this thesis describe an optical display system that integrates a deformable membrane mirror into the virtual retinal display. Analysis of the optical setup, the performance of the mirror, and results of human subject experiments are discussed. Designs incorporating the results of this research into current commercial displays is explored.

Chapter 7: Optical Design for the Monocular Display

7.1 Optical train components

The optical setup of the "true-3D" VRD allows for wavefront shaping of individual beams of light and thus the formation of different focal planes in space. See Figures 7.1 and 7.2.

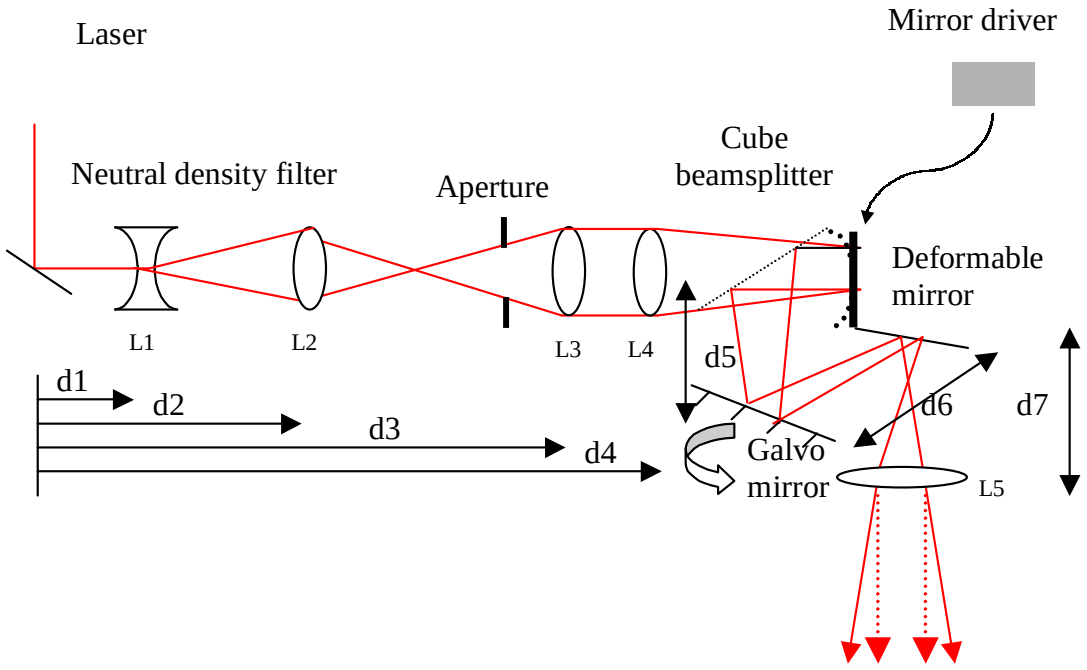


Figure 7.1. Diagram of optical setup showing an individual beam trace. When galvanometer is scanning, individual beams converge at a point beyond L_5 to form a viewing exit pupil.

Table 7.1. Lens focal lengths and locations within optical setup.

Lenses	(mm)	Distances	(mm)
L1	-20	d1	69
L2	20	d2	207
L3	100	d3	237
L4	200	d4	274
L5	60	d5	56
		d6 + d7	145

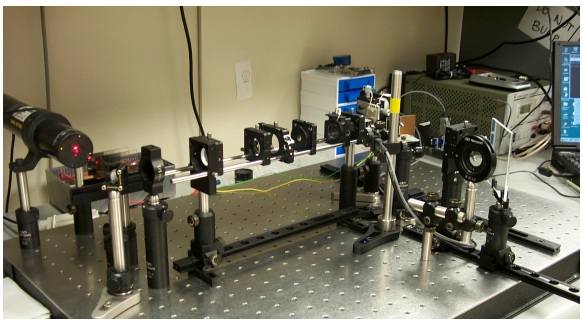


Figure 7.2. Photo of monocular optical setup.

A HeNe laser beam is expanded though L_1 and L_2 and spatially filtered. It is then collimated by positive lens L_3 and made slightly convergent by L_4. Next, the beam travels through a 50/50 cubed beamsplitter before striking a deformable membrane mirror, reflecting back through the beamsplitter and striking a scanning galvanometer mirror. The beam is then scanned through a final positive lens, L_5. This lens serves the dual function of both adjusting the divergence of individual light rays *and* converging the scanned beams to form a viewing exit pupil in space. Table 7.1 shows lens focal lengths and locations within the optical setup.

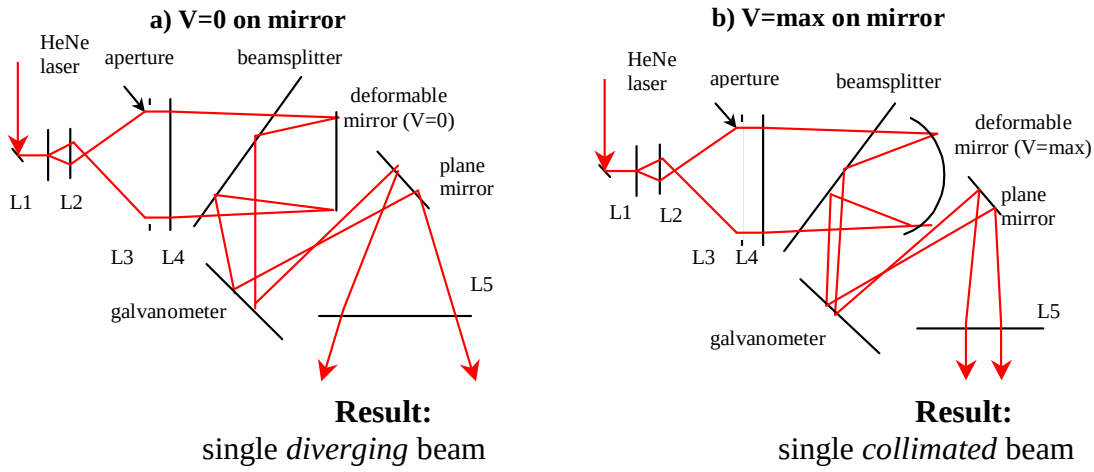


Figure 7.3. Schematic of single beam traces. *Scanned* beams converge at a point beyond L_5 to form an exit pupil.

A viewer putting his eye at the exit pupil would see a 1-D image at a focal plane determined by the amount of beam divergence (see Figures 7.3-7.5). With no voltage on the mirror this image is located at close range; at maximum voltage the image is at optical infinity. In this way the optical setup provides a range of focal planes from near to far which can be manipulated by changing the voltage on the mirror. The vertical field of view with the present optical setup is 11 degrees, a value which can be increased to a maximum of about 50 degrees by simply increasing the diameter of L_5. The diameter of light at the exit pupil in this setup can be varied from about 1 mm to 4.5 mm by adjusting the aperture. Testing with our setup was done at a beam diameter of 3.5 mm at the exit

pupil. Our future optical designs will integrate a horizontal scanner with the vertical galvanometer scanner, resulting in 2-D images with variable focal planes. This is further discussed in section 11.1.

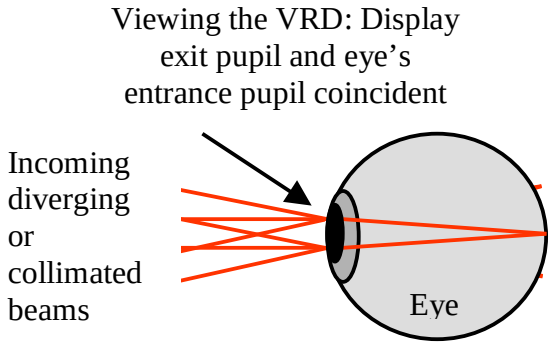


Figure 7.4. Three positions of the scanning beam illustrating the beam focused on retina.

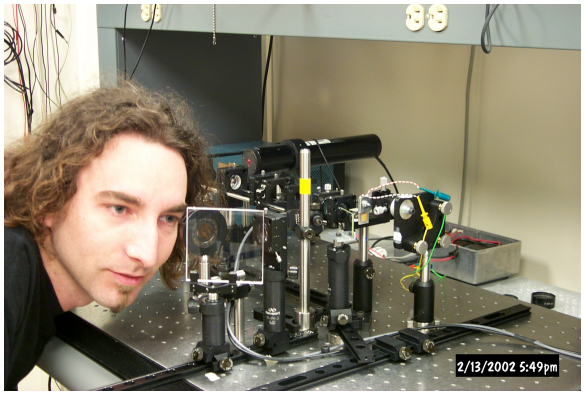


Figure 7.5. Subject viewing image through scanned display.

The deformable membrane mirror used in the setup is a MEMS device manufactured by OKO Tech. The 10-mm diameter mirror membrane is made of Si_3N_4 with a reflective coating of aluminum and is electrostatically actuated. Section 7.2 describes the mirror characteristics in detail.

The effect of deforming the membrane mirror is shown in Figures 7.6 and 7.7. Both photographs represent having the camera or viewer's eye at optical infinity while the optical power of the mirror is changed. In Figure 7.6, no voltage is applied to the mirror and the two vertical lines appear defocused because their focal plane is located close to the camera (eye). After applying maximum voltage to the mirror, the lines appear focused (Figure 7.7) because the beams entering the camera (eye) are collimated and the focal planes is at optical infinity. A viewer with relaxed accommodation and vergence would see a sharp image when maximum voltage was applied to the mirror. At smaller voltages, the viewer would see a sharp image by accommodating and verging his vision to fixation depths closer than infinity.

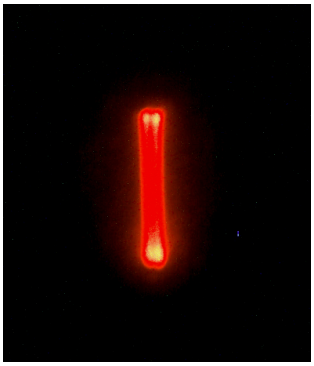


Figure 7.6. Image at optical infinity with no voltage on mirror. Since image focus is at a closer plane, the lines appear defocused at optical infinity.

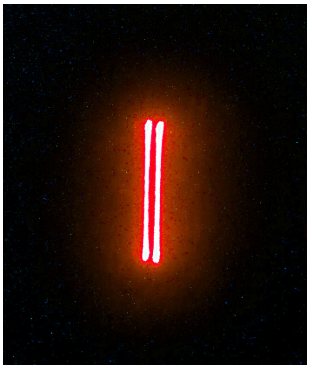


Figure 7.7. Image at optical infinity with maximum voltage on mirror. Since image focus is at infinity, image appears sharp.

7.2 Deformable membrane mirror characteristics

The MEMS deformable membrane mirror used in this study was manufactured by OKO Tech. See Figures 7.8 and 7.9. The mirror is made from a bulk micromachined silicon wafer coated with layers of Si_3N_4 (for mechanical deformation properties and electrical isolation) and Al (as the reflective surface). The structure is mounted on a printed circuit board with a circular electrode aligned beneath the membrane for electrostatic actuation. Two terminals on the PCB board allow for voltage to be applied to the mirror actuator. Table 7.2 lists the DMM specifications as given by OKO Tech. Appendix A contains the mirror operation and handling instructions supplied by OKO Tech.

Table 7.2. DMM specifications as supplied by manufacturer OKO Tech

Feature	Value
Mirror diameter	10 mm
Actuator diameter	10 mm
Focal range	0 to ≥ 2 diopters (1/m)
Control voltage range	0-300 V
Capacitance	30 pF
Cutoff frequency	1 kHz
Total dimensions with PCB board	15x15x5 mm
Membrane material	Si_3N_4
Membrane reflective coating	Al
Membrane thickness	750 nm
Density of membrane	3100 kg/m^3
Gap distance between actuator and membrane	75 um
Total mass of mirror and PCB board	≤ 5 g
Response time	< 1ms

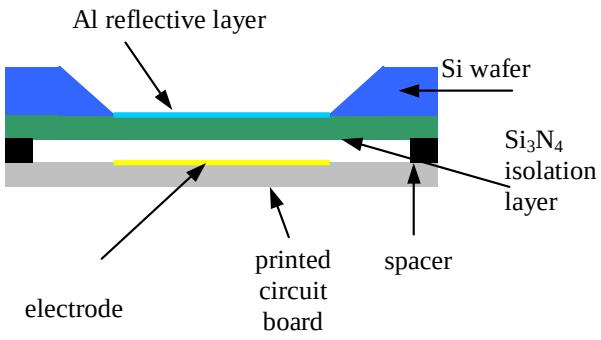


Figure 7.8. Schematic of OKO deformable membrane mirror.

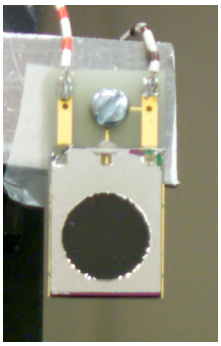


Figure 7.9. Front view photograph of mirror showing mirror, PCB board and electrical leads.

7.3 High-voltage amplifier for driving deformable mirror

To conduct dynamic measurements at controlled mirror deflection, a high-voltage amplifier has been designed that drives the deformable mirror with precise control of output voltage and frequency. Figure 7.10 shows a schematic of the main driver components of the high-voltage amplifier.

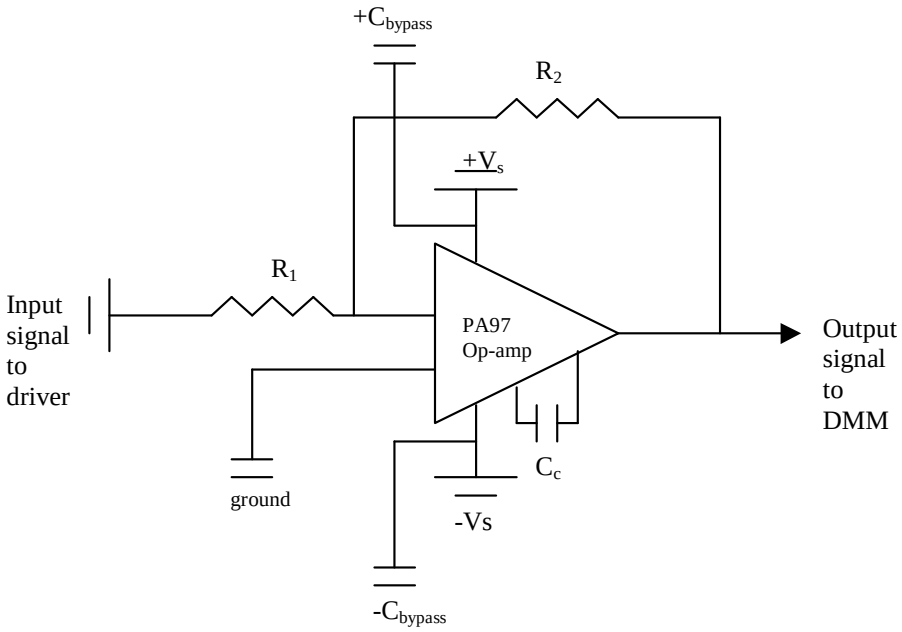


Figure 7.10. Schematic of mirror driver.

R1 and R2 comprise the gain of the amplifier:

$$GAIN = -\frac{R1}{R2}$$

In the design of this driver the resistor values are R1= 440 kΩ and R2= 3.9 kΩ; therefore

$$GAIN = -\frac{440}{3.9}$$

$$= \mathbf{-112}$$

The data sheets for the Apex PA97 op-amp used in the driver can be found at: http://www.apexmicrotech.com/pdf/power_op_amps/pa97.pdf. The data sheet graphs indicate amplifier roll-off at 3 kHz and a bandwidth of 8 kHz at our required maximum

output voltage of 300 V. At lower output voltages, however, the driver can operate at higher bandwidths. This driver may also be modified in the near future to provide higher bandwidths at high voltages.

7.3.1 Static operation of mirror

The mirror operates statically when a DC voltage is fed to the driver. This allows for the mirror to deflect and remain in the deflected state until the voltage is no longer applied. An input DC voltage to the driver is amplified –112 times:

$$\mathbf{V_{mirror} = -112 * (DC\ voltage\ to\ driver)}$$

The mirror requires a positive voltage; therefore the DC voltage fed to the driver should be negative because gain is negative. For example, an input DC voltage of -2V would give an output voltage of 224 V to the deformable mirror.

7.3.2 Dynamic operation of mirror

To operate the mirror dynamically, both an AC and a DC signal are required. The required DC offset is equal to one-half the negative peak-to-peak AC voltage:

$$\mathbf{DC\ offset = -1/2\ (AC_{pp})}$$

One must be careful in both static and dynamic operation of the mirror that the maximum voltage range of the mirror is not exceeded. Overshoot of this voltage can cause the mirror to snap down to the electrode, causing damage or shattering the mirror membrane. Appendix B shows DC voltages for static operation of the mirror as well as AC and corresponding DC voltages for dynamic operation of the mirror. Appendix C shows the mirror driver power-up procedure.

Chapter 8: Static testing of deformable mirror

8.1 Mirror optical power outside of setup

The optical power of the mirror was first tested with the mirror outside of the optical setup (raw optical power). A simple setup with a laser beam striking the mirror membrane was used, and optical power was measured by finding the location in space of the smallest diameter of the reflected beam using a beamsplitter. With no voltage applied to the mirror, the surface remains flat and the focal point is located at infinity. With voltage applied to the mirror, the focal point is formed at a point in space between the mirror and infinity. As specified by OKO Tech, voltage greater than 300 V was not applied in order to avoid the risk of electrostatic snapdown. Table 8.1 tabulates the applied voltage on the mirror versus the optical power.

The mirror reached a maximum raw optical power of 0.97 diopters at 300 V. Other deformable mirrors tested in the laboratory from the same manufacturer reached optical powers as high as 1.8 diopters. Although the specification from OKO calls out a 2-diopter focal range, the actual focal range among mirrors can be quite variable and depends on the MEMS microfabrication process. Mirrors can exhibit variation in performance based on differences in membrane tension, layer thicknesses, and gap distances between the membrane and the electrode.

Table 8.1. Mirror raw optical power

Applied Voltage	Beam focus (m)	Beam focus (diopters = 1/m)
0	infinity	0.00
100	2.31	0.43
200	2.00	0.50
225	1.55	0.64
250	1.40	0.72
275	1.20	0.83
285	1.11	0.90
295	1.06	0.95
300	1.03	0.97

8.2 Mirror optical power within the setup

Although the mirror's raw optical power would not meet our goal of a 0-3 diopter range display, an optical setup was created that increased the mirror's effective optical power significantly. The deformable mirror was placed within the optical setup as shown in Chapter 7, Figure 7.1, repeated here for reference as Figure 8.1.

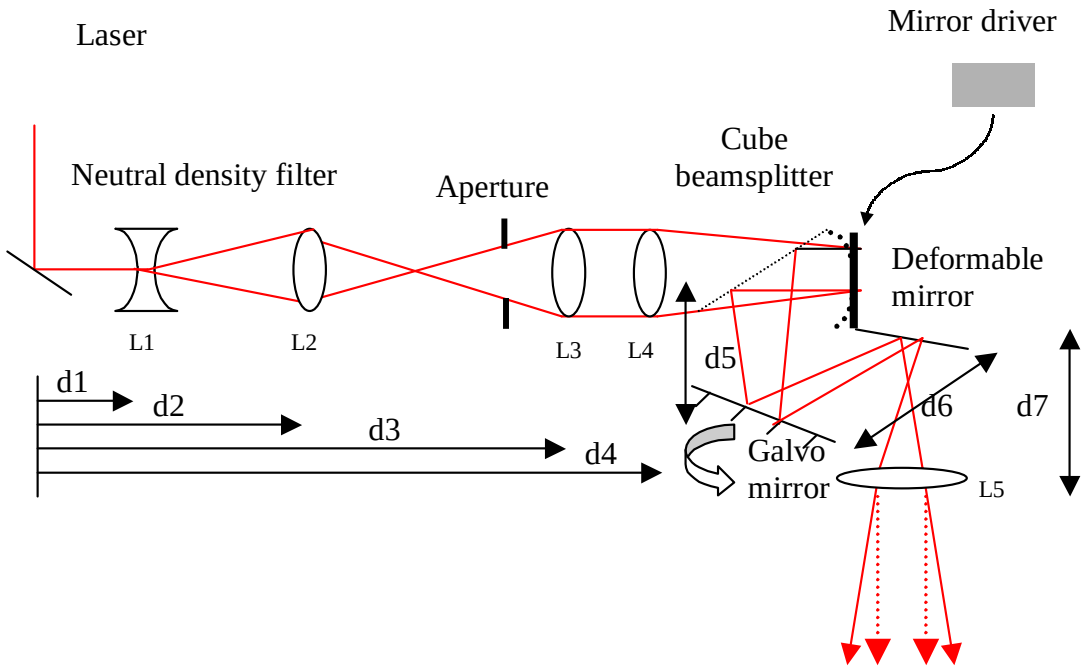
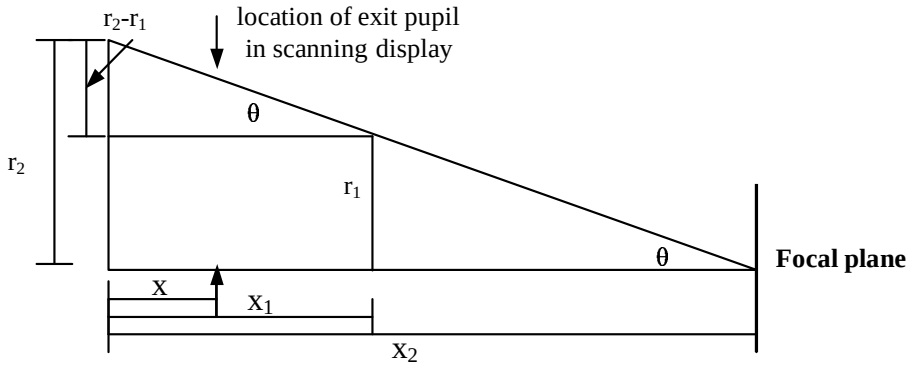


Figure 8.1. Diagram of optical setup (repeated from Figure 7.1).

8.2.1 Measurements with beam profiler

To quantitatively measure the mirror's optical power within the setup, a beam profiler (manufactured by Thorlabs, Inc.) was used to measure the diameter of the beam after it passed through the final viewing optic L_5. During this experiment the galvanometer was not in scanning mode, so that the output was a stationary circular beam. The beam radius was measured at two different points in space (r_1 and r_2) and the focal plane was back-calculated knowing the distance between the measurements and the location of the exit pupil. Below is the calculation showing this method.



Known: r_2, r_1, x, x_1

focal plane distance from exit pupil = x_2 - x

where $x_2 = r_2 / \tan \theta$

and $\theta = \tan^{-1} ((r_2 - r_1 / x_1))$

The optical setup was found using beam profiling to produce a focal range of 0 to 3.1 diopters with an applied voltage range of 0-300 V (see Figure 9.1). This focal range could be brought forward in space by moving L_5 in small increments, producing images closer than 3 diopters but with the most distant image appearing at less than infinity. In one configuration of this type, used in the following human subject experiment, the optical range was 0.57 to 3.83 diopters. Figure 8.2 summarizes the mirror raw optical power and its optical power within the optical setup.

Table 8.2. Focal point of light striking the deformable mirror within optical setup at various mirror voltages.

Voltage (V)	Focus in diopters (1/m)
300	0
230	1.3
0	3.1

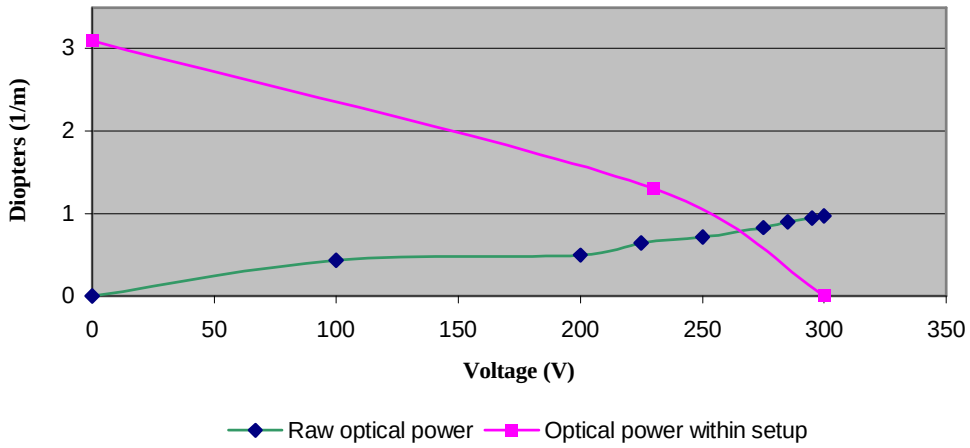


Figure 8.2. Applied voltage on mirror and corresponding optical power. The mirror has a maximum raw optical power of 1 D and maximum power within the setup of 3 D. Within the optical setup, there is a reverse relationship so that when maximum voltage is applied to the mirror, the focus is at 0 D.

8.2.2 Human subject experiments

A group of 10 human subjects were evaluated in order to compare actual eye accommodation when viewing the display with the focal range found using the beam profiler. In this experiment the galvanometer was turned on to scanning mode, so that a viewing exit pupil was formed at a point beyond L_5. A viewer putting his eye at the exit pupil would see a 1-D image at a focal plane determined by the amount of beam divergence (see Figures 7.3, 7.6, and 7.7). With no voltage on the mirror this image was found with beam profiling to be located at 3.83 diopters (0.26 m); with maximum voltage on the mirror the image was at 0.57 diopters (1.75 m).

Testing was done in a dark room and subjects (HIT lab co-workers) viewed the monocular display with their left eye (the right eye was not patched). Five minutes were reserved for dark-adaptation before the experiment began, after which a practice session was conducted to allow subject familiarization with the display. The distance that the scanned image was located in space from the viewer's eye was varied and a laser

autorefractor was used to measure subjects' accommodation while fixating on the scanned image at three different focal planes.

The autorefractor takes a reading of both the spherical and cylindrical power of the eye. Because autorefractors will sometimes mistake spherical power for cylindrical power, the spherical equivalent (SE = spherical power + ½ cylindrical power) is generally used in opthalmological literature as a better estimate of the true spherical power of the lens. The setup produced an average SE fixation range of –3.35 +/- 0.70 to -0.70 +/- 0.51 diopters (30 cm to 143 cm). Table 8.3 shows the data for each subject and Figure 8.3 plots the average experimental SE along with the corresponding expected fixation plane found with the beam profiler. The expected spherical equivalent values are within one standard deviation (SD) of the experimental values. Data for each subject was normalized by adding or subtracting a constant from all data points to account for autorefractor error.

Table 8.3. Accommodation data taken from 10 human subjects accommodation to scanned image at three different focal planes.

	Accommodation Plane		
	Near	Mid	Far
SM	-2.94	-1.37	0.10
MF	-2.71	-1.80	-0.70
CB	-4.79	-1.51	-0.40
JC	-2.71	-1.73	-1.64
SF	-4.15	-2.99	-1.21
RB	-3.74	-2.98	-1.07
NH	-3.57	-2.01	-0.43
RM	-2.79	-2.05	-0.40
NS	-3.23	-2.34	-0.99
BS	-2.89	-2.22	-0.32
Average SE	**-3.35**	**-2.10**	**-0.71**
Expected SE	-3.83	-2.19	-0.57
Std Dev (n-1)	0.70	0.55	0.51

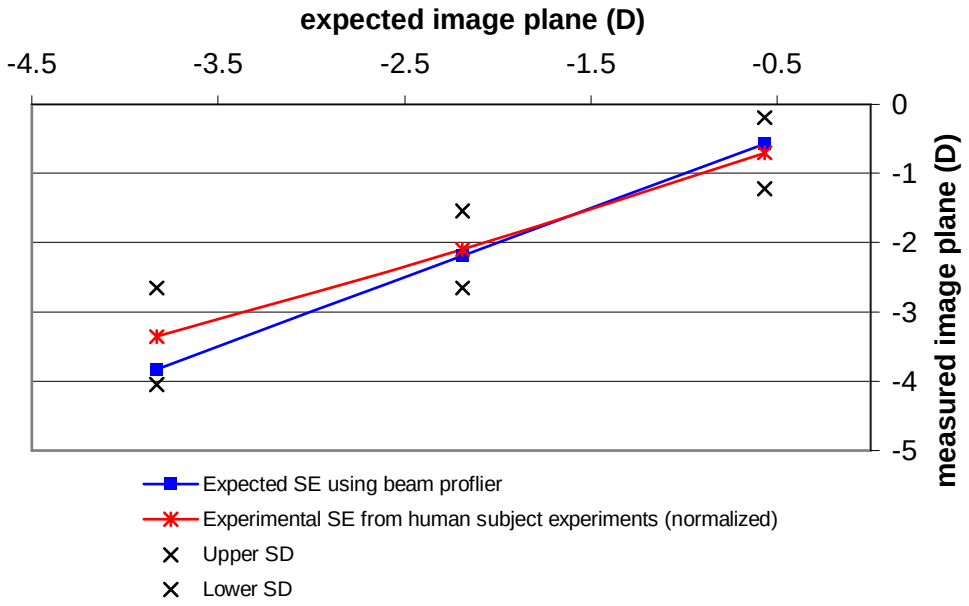


Figure 8.3. Average spherical equivalent of 10 subjects' accommodation to variable-focus VRD (experimental SE) and experimental spherical equivalent found with beam profiler (expected SE).

8.3 Visual changes in the display at various focal planes

While the DMM allows for the creation of images at various focal planes, an additional undesirable phenomenon occurs due to the parabolic curvature of the mirror. The x-y size of an image is *magnified* as it moves away from the viewer, whereas in normal viewing objects that are far away are smaller than objects up close. This effect is called "anomalous perspective" and was a characteristic mentioned by Mills et al. (1984) in their paper on a vibrating-mirror 3D display. It is noted, however, that despite this phenomenon, human subjects in our experiment still exhibited the expected changes in accommodation and vergence to various stimuli. Anomalous perspective is a pictorial cue issue, not a mechanical one, and an adjustment through software or analog circuitry would be used to compensate for the phenomenon.

Chapter 9: Dynamic testing of deformable mirror in ambient air pressure and high vacuum

The dynamic properties of the DMM are integral to this project, as the operational speed (bandwidth) of the DMM plays a key part in the modulation speed of the scanned light display. For example, each pixel in the scanned image display appears at a certain focal plane in space. For pixel-by-pixel modulation, the mirror membrane would need the potential to deflect at a different distance to alter the wavefront of each pixel in the display as it was scanned. The capacity of the mirror to meet this challenge based on the data presented in this section is discussed further in Chapter 11.

Dynamic measurements were conducted on the mirror using the driver amplifier discussed in section 7.2.2. Mirror deflection and frequency were controlled by feeding the mirror a certain input voltage and frequency from the driver. The mirror's deflection in response to the signal was measured with a Polytec OFV-303 vibrometer, which measures the dynamic Doppler shift of laser light reflecting off the membrane and produces an analog vibration signal, measured on an oscilloscope. The mirror was tested in both ambient air and vacuum to see whether any increase in bandwidth could be attained when air damping was not present.

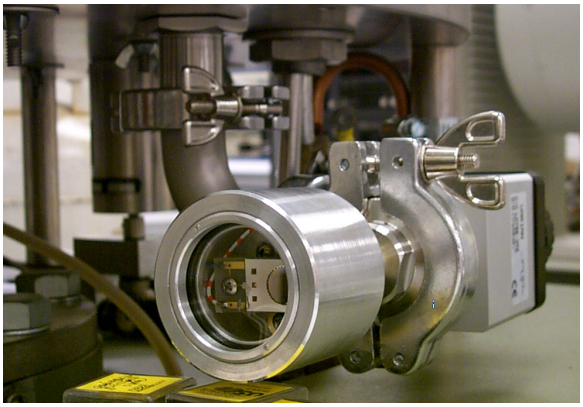


Figure 9.1. Deformable mirror being tested under high vacuum.

To conduct testing in vacuum, a vacuum chamber with a high-quality optical flat was machined from aluminum stock (see Figure 9.1). The chamber was pumped down using an electron-beam physical vapor deposition system pump to 1.9e-6 Torr, classified as high vacuum (Varian, 1992). Testing of the mirror was conducted immediately after pumpdown to

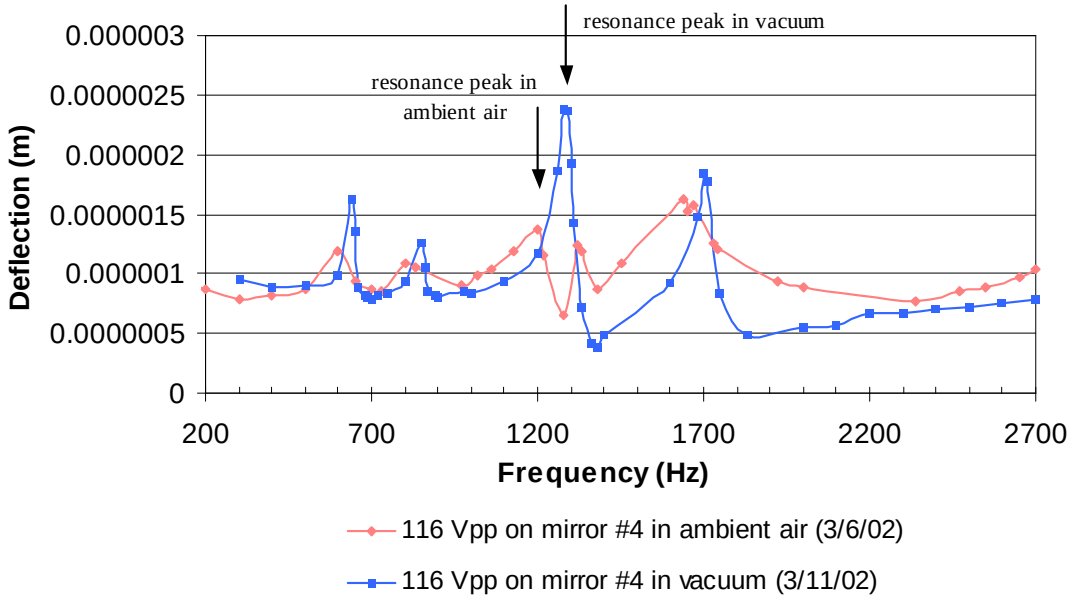


Figure 9.2. Frequency response curve of deformable mirror.

avoid changes in chamber pressure due to outgassing or leakage. The first few data points taken at the commencement of testing were repeated at the end of the experiment with the same results, indicating that no significant changes in chamber pressure had occurred.

Because only one mirror was available in laboratory stock for vacuum testing, a relatively small peak-to-peak voltage (116 Vpp) was fed to the mirror to avoid the risk of snapdown at resonance. Data was taken up to a maximum frequency of 2.7 kHz, both to avoid unexpected breakage at higher frequencies and because specifications from mirror manufacturer OKO Tech stated a cutoff frequency of 1 kHz.

Figure 9.2 shows the mirror response in ambient air and in vacuum. The frequency response curve in vacuum is shifted slightly to the right, showing a slight increase in bandwidth of about 80 Hz. An increase in amplitude (or membrane deflection) of about double is seen in vacuum compared to ambient air. A sharp peak is seen in ambient air at

1200 Hz. This data supports specifications given by manufacturer OKO that the first resonant frequency occurs at about 1 kHz.

Slight increases in amplitude are seen on both curves at around 600 and 800 Hz; according to OKO Tech these may be due to the mirror architecture. The actuator PCB board is epoxied to only two corners of the MEMS mirror rather than to all four corners; this may be causing cantilever-like vibrations at certain frequencies. Additional twisting and bending of the membrane supporting structure could also be the source of these peaks. In summary, the mirror gains about 80 Hz bandwidth in vacuum compared to ambient air. For the purposes of this project, 80 Hz of added frequency is probably not worth the added complexity of packaging the mirror in vacuum. The frequency response curve is further explored in sections 10.3 and 10.4.

Chapter 10: Modeling the deformable membrane mirror

This chapter discusses the characteristics and theoretical performance of the OKO Tech deformable mirror used in this study based on membrane and electrostatic theory. The analysis draws from a paper by Grosso and Yellin (1977) and membrane theory by Morse (1948). Grosso and Yellin found high correlation between measured data from their membrane mirror and membrane theory drawn from Morse. A number of other authors have used the membrane model in their analyses of deformable mirrors (Vdovin and Sarro, 1995, Mansell, 1998, Burley et al., 1998).

There is also argument for modeling the mirror as a thin plate (shell) instead of a membrane because the mirror plus its supporting structure may exhibit bending stiffness and internal stresses. The ideal mechanical model for a plate assumes only a bending restoring force, but no internal stresses. The plate approximation is only valid if the plate is bending less than its thickness and the plate is under negligible internal stress (Mansell, 2002). In our case the deflection of the mirror is greater than the mirror thickness; thus, the membrane model is used. It is noted, however, that the model of an ideal membrane assumes that bending stresses are negligible and may present a source of error.

10.1 Finite element model

The deformable mirror deflects parabolically above the electrode when a voltage is applied. Figure 10.1 is a finite element model of the membrane when 300 V is applied to the electrode. The model was generated with software from Intellite, Inc.

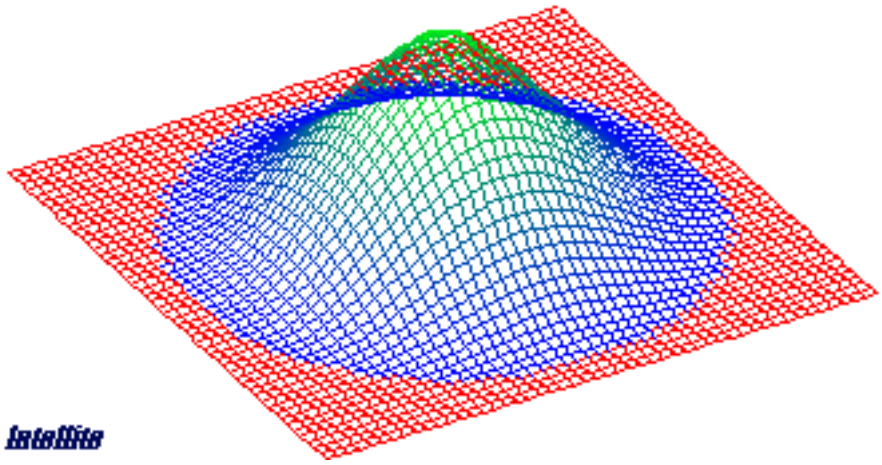


Figure 10.1. FEA model of deformable mirror at 300 V applied voltage.
FEA modeling software courtesy of Intellite, Inc.

10.2 Calculation of electrostatic force and membrane tension

Theoretical analysis of the mirror allows us to calculate the force on the membrane and the resulting membrane tension. Membrane tension can then be used to calculate the resonance frequencies of the membrane and compare them to results found experimentally.

The DMM used in this study is electrostatically actuated by an electrode with the same diameter (10 mm) as the membrane. The shape of the deflection of a membrane mirror is given by solving (Morse, 1948),

$$\nabla^2 Z = -\left(\frac{F(r,\theta)}{T(r,\theta)}\right) \qquad \textbf{(1)}$$

Where Z is the mirror surface, $F(r,\theta)$ is the force distribution, and $T(r,\theta)$ is the membrane tension. The steady-state deflection of a membrane with a distributed force at its center with respect to radius r is given by,

$$z(r) = \frac{F}{2\pi T}\left[\ln\left(\frac{R}{S}\right) + \frac{1}{2S^2}\left(S^2 - r^2\right)\right] \qquad 0<r<S$$

$$z(r) = \frac{F}{2\pi T}\left[\ln\left(\frac{R}{r}\right)\right] \qquad S < r \le R \qquad \textbf{(2)}$$

where S is the actuator radius, R is the radius of the membrane, r is the distance from the center of the membrane, T is the tension on the membrane, and F is the force on the membrane. See Figure 10.2.

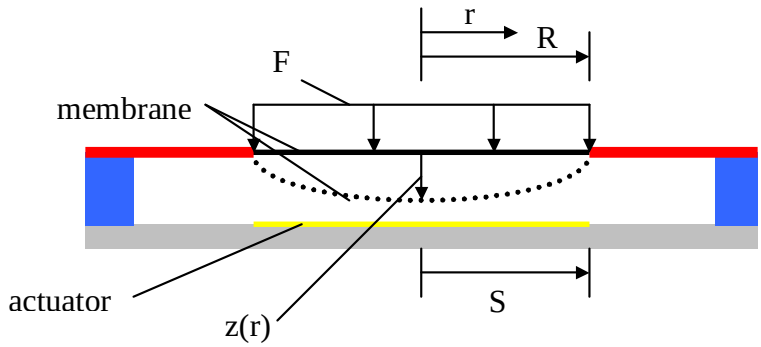


Figure 10.2. Diagram showing values used in membrane deflection calculation.

When the actuator radius is equal to the membrane radius, and at the center of the membrane, the equation simplifies to

$$z(r) = \frac{F}{2\pi T}\left(\frac{1}{2}\right) \qquad \textbf{(3)}$$

It is important to remember that equations (2) and (3) are only valid for an actuator located in the center of the membrane. An off-center location requires a numerical solution to the equations.

The electrostatic force between a pair of parallel plates is given by (Grosso and Yellin, 1977),

$$F(V) = \frac{e_0 e_r A V^2}{2(d-z)^2} \quad \textbf{(4)}$$

where e_o is the dielectric constant of free space (e_o = 8.85 x 10^{-12} F/m), e_r is the dielectric permittivity of air (e_r =1), A is the area of the electrode, V is the applied voltage, d is the total distance between the electrode and the undeflected membrane, and z is the membrane deflection.

Table 8.1 lists the mirror raw optical power in response to an applied voltage. Using this data, the corresponding deflection can be calculated using the equation for a parabola (Beyer, 1987):

$$y = \frac{x^2}{4f} \quad \textbf{(5)}$$

where y is the depth of the parabola, x is the distance from the vertex of the parabola, and f is the focal length. In our case, y is the membrane deflection (z) and x is the mirror radius (r). We will thus change the variables to

$$z = \frac{r^2}{4f} \quad \textbf{(6)}$$

We can now solve for the tension in the membrane knowing the deflection from equation (6) and the electrostatic force from equation (4). Solving for tension in equation (3),

$$T = \frac{F}{4\pi z(r)} \quad \textbf{(7)}$$

We now substitute the range of voltages and corresponding foci from Table 8.1 into (6) to find a range of deflections z, and then substitute these z into (4) to calculate a range of electrostatic forces F. These F are then substituted into (7) to calculate a range of membrane tensions. Tables 10.1 and 10.2 list known values and results of these calculations.

Table 10.1. Known values used in calculation of membrane tension.

radius of membrane (m)	0.005
maximum optical power (m)	1
area of membrane (m^2)	7.85398E-05
gap distance (m)	7.50E-05
Er (F/m)	1
E0 (F/m)	8.85E-12
thickness (m)	7.50E-07
density of membrane (kg/m^3)	3.10E+03

Figure 10.3 is a plot of applied voltage vs membrane tension. Tension increases with voltage because the electrostatic force on the membrane increases as the membrane deflects and gets closer to the electrode. Membrane tension increases an additional amount due to stretching. These two effects create a complex tension field and result in a nonlinear mirror response to force.

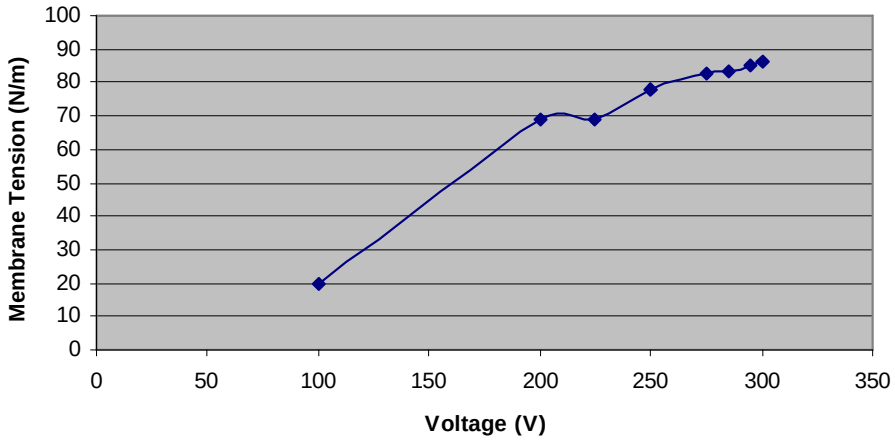


Figure 10.3. Applied voltage on mirror vs. membrane tension

10.3 Theoretical frequency response

Theoretically, the deformable membrane mirror operates linearly until its first resonant frequency is reached, beyond which the frequency response becomes nonlinear. Thus there is a cutoff frequency that defines the maximum bandwidth of the mirror. The resonance frequencies of a circular membrane in the 0^{th} order angular modes is given by (Morse, 1948)

$$\nu_{0n} = \frac{\gamma_{0n}}{2a}\sqrt{\frac{T}{\sigma}} \qquad \textbf{(8)}$$

$$\gamma_{0n} = \beta_{0n} + \frac{2\chi}{\pi^4 \beta_{0n}{}^3} \qquad \textbf{(9)}$$

where γ_{0n} is the resonant frequency of the nth radial mode, T is the tension per unit length (or stress-thickness product) of the membrane, σ is the mass per unit area of the membrane, β_{0n} is the root values of the Bessel function of the 0^{th} order, and χ is a measure of the relative importance of the restoring force due to air confined behind the membrane.

When the membrane is enclosed in a vacuum, the second term in (9) disappears because χ=0. The value of the Bessel function for the first radial mode γ_{00} is 0.7655 (Morse, 1948). The equation for the first resonant frequency of a membrane in vacuum therefore becomes

$$\nu_{00} = \frac{0.7655}{2a}\sqrt{\frac{T}{\sigma}} \qquad \textbf{(10)}$$

$$\text{or} \quad \nu_{00} = \frac{0.7655}{2a}\sqrt{\frac{stress}{density}} \qquad \textbf{(11)}$$

Knowing the membrane tension (section 10.2), we can now calculate the first resonant frequency in vacuum. Table 10.2 shows the values used to calculate first resonant frequency at various voltages. Figure 10.4 is a plot of voltage vs. first resonant frequency. First resonant frequency increases with increasing applied voltage because of the increasing tension on the mirror membrane. The plot of applied voltage vs. tension (Figure 10.3) follows the plot in Figure 10.4 because the membrane tension and first resonant frequency differ only by a constant.

Table 10.2. Values used in calculation of theoretical first resonant frequency in vacuum

Applied V	Deflection z (m)	Elec. force F_e(N)	Tension T (N/m)	Stress (Pa)	1st res. freq. (Hz)
100	2.70E-06	6.65E-04	19.57	2.61E+07	7.02E+03
200	3.12E-06	2.69E-03	68.59	9.14E+07	1.31E+04
225	4.03E-06	3.49E-03	69.02	9.20E+07	1.32E+04
250	4.47E-06	4.37E-03	77.68	1.04E+08	1.40E+04
275	5.20E-06	5.39E-03	82.56	1.10E+08	1.44E+04
285	5.62E-06	5.86E-03	83.03	1.11E+08	1.45E+04
295	5.91E-06	6.34E-03	85.28	1.14E+08	1.47E+04
300	6.09E-06	6.59E-03	86.12	1.15E+08	1.47E+04

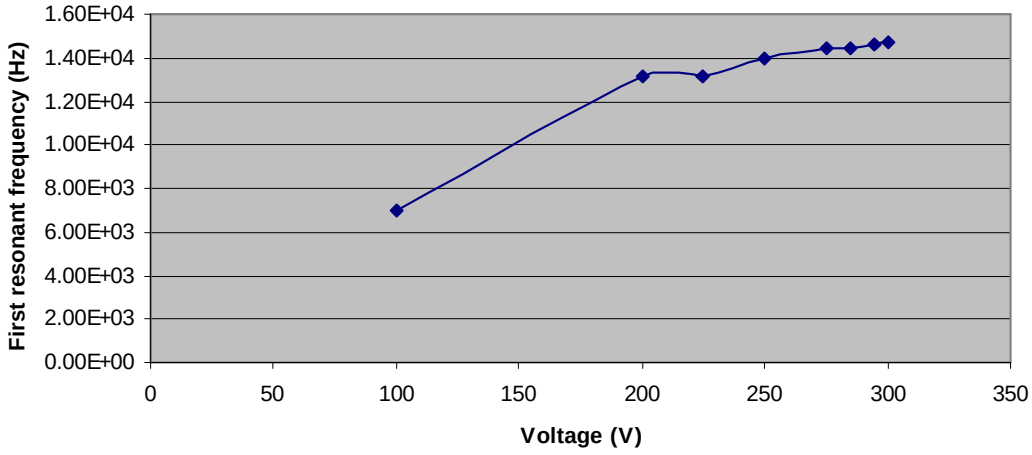


Figure 10.4. Applied voltage on mirror and corresponding theoretical first resonant frequency in vacuum.

10.4 Comparison of experimental results with theory

Comparing the two sets of data on Figure 10.5 (repeated for reference from Figure 9.2), it is observed that resonance frequency peaks under vacuum (undamped) are at a slightly higher frequency than resonance peaks in ambient air (damped). This agrees with vibration theory (Beachley and Harrison, 1978), which states that the damped natural frequency ω_d is less than the undamped natural frequency ω_n for systems under damped free vibration. There is also an increase in amplitude of about double in vacuum compared to ambient air.

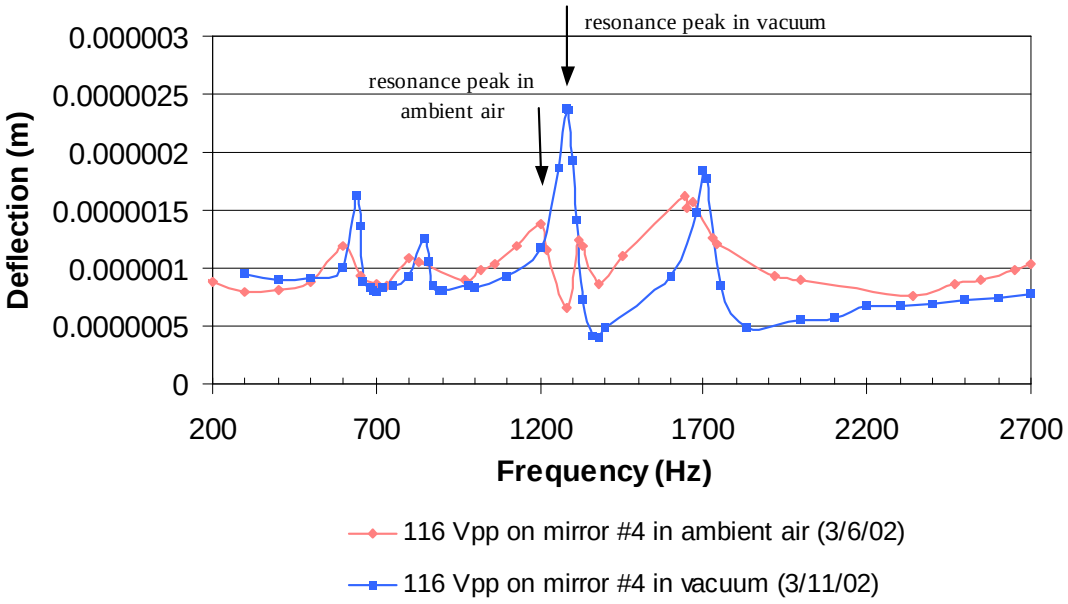


Figure 10.5. Frequency response curve of deformable mirror (repeated for reference from Figure 9.2).

To compare the theoretical resonant frequency with the resonant frequency found experimentally, we look at the resonant frequency on Figure 10.4 corresponding to the voltage applied during the experimental frequency response analysis, 116 V. Figure 10.4 shows the theoretical first resonant frequency at 116 V to be about 7.5 kHz. Our experimental analysis was taken only to 2700 Hz for two reasons: (1) to avoid mirror breakage, as the devices cost $1000 each and the mirror under analysis was the only one

available in the laboratory at the time, and (2) specifications from manufacturer OKO Tech stated a cutoff frequency of 1 kHz, which was confirmed in our experimental analysis showing large amplitude peaks around this frequency. The frequency response curve in Figure 10.5 of the mirror in vacuum shows a large amplitude peak at 1280 Hz.

The resonant peak at 1280 Hz, as well as the other, smaller, peaks seen on Figure 10.5 are likely due to the resonances of the membrane plus its supporting structure. When the mirror membrane is actuated by the electrode beneath it, the membrane deflects in response; however, the supporting structure around the membrane also deflects to some degree. See Figure 10.6. The membrane alone has a theoretical first resonance at 7.5 kHz, but the entire structure has a first resonance at some lower frequency, resulting in a complex combined frequency response. Our results show that a combined plate/membrane model might fit the experimental data more closely, as the membrane model assumes bending stresses are negligible. Further analysis using an FEA program such as ANSYS could be used create this kind of model.

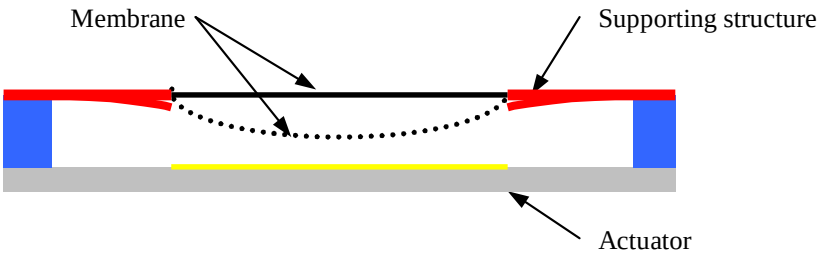


Figure 10.6. Schematic of deformable mirror showing possible dynamic structural response of mirror membrane and its supporting structure. Though the membrane alone has a theoretical first resonance at 7.5 kHz, the entire structure has a first resonance at some lower frequency, resulting in a complex combined frequency response.

Another potential source of discrepancy between theoretical and actual data is the membrane tension used in calculating first resonant frequency. The tension formula assumes that the membrane deformation is a perfect parabola. This is not possible in

reality since the membrane has a fixed outer boundary and the actuator has more effect on the center of the membrane than the outer edges. Experimentally, tension in the mirror membrane can only be determined destructively by etching the membrane and measuring the resulting surface curvature, preventing any further analysis on the mirror. Thus assumptions must be made during theoretical calculations, which may be a source of error.

Chapter 11: Discussion and future work

Table 11.1 is a summary of the characteristics of the monocular display described in this thesis.

Table 11.1. Monocular display characteristics

Focal range	0 to 3 diopters
Size of exit pupil	3.5 mm
Field of view	Up to 50 degrees, vertical
Color	Monochrome red
Image produced	1-D line scan with variable focus
Bandwidth of deformable mirror	1100 Hz in ambient air 1280 Hz in vacuum
Resolution	To be determined in future work

11.1 Expansion to bi-ocular display

There are a number of additions currently being made to the optical setup to expand it to a bi-ocular system with x-y scanning and variable focus. See Figures 11.1 and 11.2. The system provides two identical images (one to each eye) while being adaptable to the vergence angle of the eyes. For instance, when the observer is fixating a spot in space, the beamsplitters are rotated in equal and opposite directions to align the scanned image with the vergence angle of the eyes. These beamsplitters are mounted on a linear translation rail in order to adjust for each person's inter-pupillary distance. The observer views the image reflected from beamsplitters so that the images can be superimposed onto real world objects for augmented viewing.

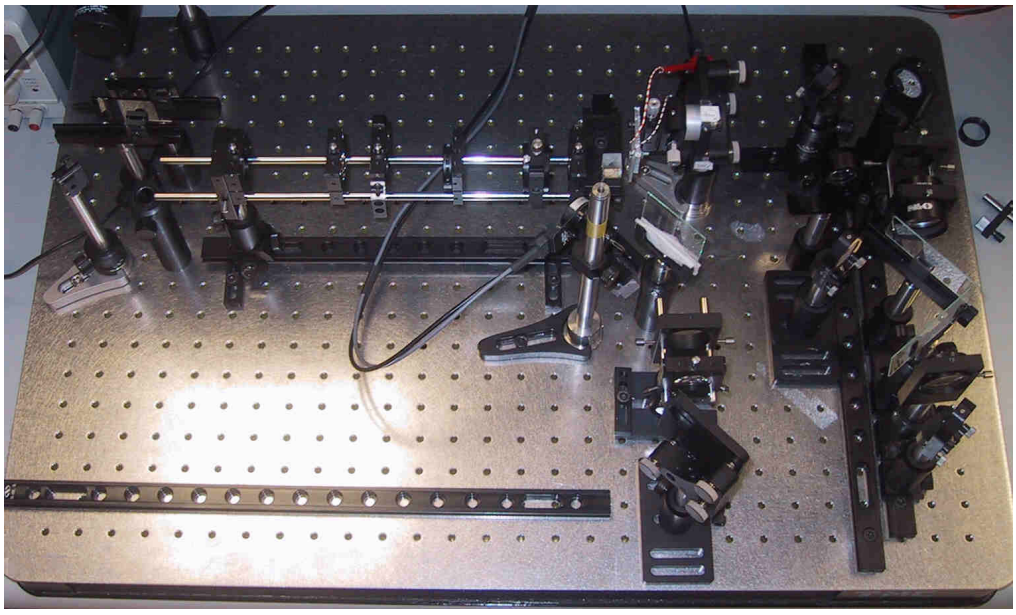


Figure 11.1. Photograph of bi-ocular retinal light scanning display

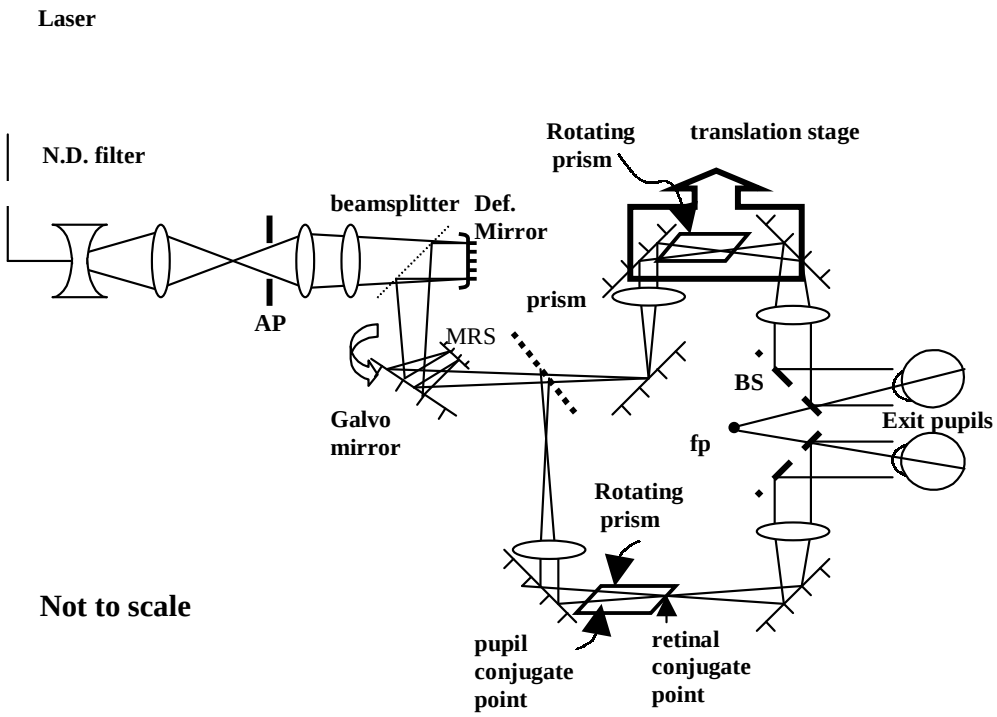


Figure 11.2. Schematic of bi-ocular retinal light scanning display

A canning polygon galvanometer is being incorporated to complete a 2D scan. The scan rate for the VRD is found by multiplying the number of lines in the display by the refresh rate of the display. In the original design for a commercial retinal scanning display developed at the HIT lab (Johnston and Willey, 1995), a mechanical resonant scanner was built and patented that was used in conjunction with a galvanometer mirror, allowing the optical beam to undergo a double bounce off the two mirrors. This allowed for an increase in the optical scan angle and a final display resolution of 640 pixels by 525 lines, refreshed at 60 Hz. Fields of view up to 50 degrees were accomplished. Our present system will be able to achieve these same results if the same arrangement of optical components is used.

The bi-ocular setup will eventually be expanded to a binocular system that presents stereoscopic images. The binocular system will present two different images to the eyes that allow accommodation and vergence to occur, just as in everyday natural human vision. The binocular system will be used to compare the importance of accommodative depth cues with standard stereoscopic (retinal disparate) depth cues.

11.2 Challenges

Depth-modulation rate will be a significant issue in future designs. The limiting factor for display resolution is the speed at which the deformable mirror can operate. The bandwidth of the deformable mirror determines how quickly the depth of scanned pixels within an image can be changed.



Figure 11.3. DMM manufactured by Intellite, Inc. to be investigated for future designs.

We have received a new MEMS deformable mirror from Intellite, Inc. that is half the diameter (5 mm), has the same amplitude range, and has a higher operating frequency than our current mirrors from OKO Technologies (see Figure 11.3). The main advantages

of the Intellite mirror are a higher resonant frequency (manufacturer Intellite specifies 26 kHz versus OKO Tech's 1 kHz), and comparable optical power at lower voltages (2/3 the voltage of the OKO mirror). Specific mirror characteristics are discussed in the paper, "Micromachined Silicon Deformable Mirror" written by Intellite founder Justin Mansell (1998). The Intellite mirror will be investigated further in the near future.

A pixel-by-pixel modulated system would be the "gold standard" of a display of our type, since with this method the wavefront of each individual pixel could be modulated to a certain depth in space every time it was scanned. However, this kind of modulation would require extremely high bandwidth of the deformable mirror used to manipulate the wavefront. For VGA output, the mirror would need to operate at:

(800 lines) x (600 pixels/line) x (60 Hz) = **28.8MHz**

This is obviously unattainable with present mirror bandwidths. Another design option is to create a display with graded planes of depth, where whole rectangular fractions of the display would display different depths. See Figure 11.4. In this configuration the mirror would operate at maximum bandwidth to switch depths between sections. This kind of display is useful for further human subject testing and could be done simply with the addition of another scanner, but would be impractical for a truly compelling 3D display.

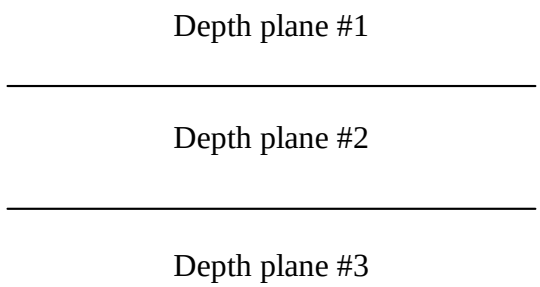


Figure 11.4. Example of display configuration with blocked planes of depth using a graded response from deformable mirror.

One option for utilizing present mirror bandwidths is to operate two or more mirrors in series to multiply the effective bandwidth and focal range by some factor. Another option is to use a different type of scan. A calligraphic scan, for instance, might refresh display pixels in the order of near to far depth planes, the mirror only changing shape when the focal plane advanced. Other design options dealing with the challenge of mirror bandwidth are being actively explored but are confidential at present due to patent activity.

11.3 Use of a deformable mirror in a non-scanning display

Although the use of a deformable membrane mirror is best for scanned light displays because individual beams of light can be modulated, it might be useful in other configurations such as LCD displays. A deformable mirror the size of the display screen could be mounted in front of the display pixels. Assuming sufficient bandwidth of the mirror and liquid-crystals, the focal plane of certain areas of a scene could be changed in succession. See Figure 11.5.

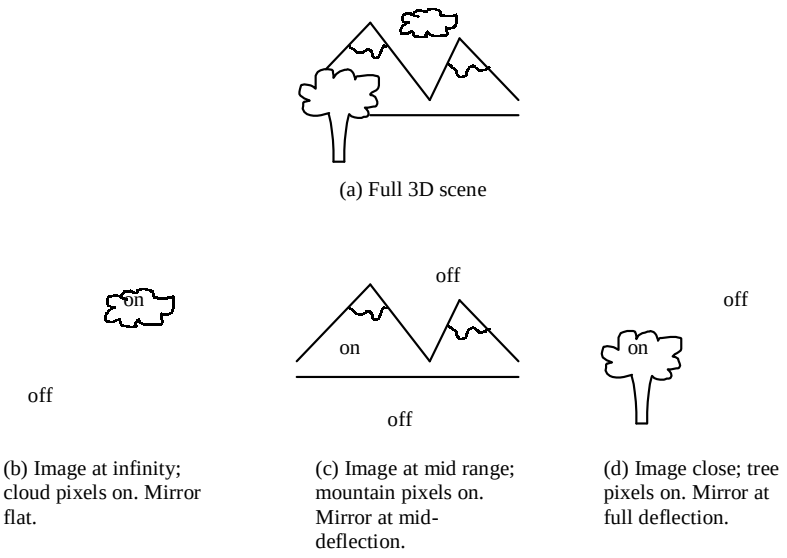


Figure 11.5. Design for an LCD display screen utilizing a DMM. The images at various depth planes would be refreshed with the deformable mirror at the appropriate deflection.

Scene (a) shows a cloud at optical infinity, mountains at some mid range distance, and a tree at close range. To render this image on an LCD with a deformable mirror, the pixels at a certain depth plane would be turned on while the rest of the scene pixels were off. The mirror would then change deformation to a different plane in space and the pixels at that plane would be turned on while the rest were turned off, and so on. This technique could render a 3D image if done at a high enough refresh rate for both mirror deflection and LCD pixel modulation. The technique would probably work even better using a head-mounted LCD display because the display screen and mirror membrane would be smaller, making faster mirror bandwidths possible.

Chapter 12: Conclusion

A monoscopic optical bench has been developed that can manipulate the wavefront of light at greater than video frame rates. The display is being used to compare human visual performance using the natural linked depth responses of accommodation and vergence, whereas current commercial stereo displays require that this natural response be decoupled. The present display projects a 1-dimensional monochromatic line scan with variable focus and up to a 50-degree field of view. Clinical studies have been conducted to measure human visual response to the displayed images. A focal range of 0 to 3.2 diopters was achieved, verified with laboratory beam profiling data and human subject data. Frequency analysis was conducted on the mirror in both ambient air and vacuum conditions. The performance of other mirrors with different design architectures will be investigated in the near future. Work is currently underway toward the building and testing of a full-color, bi-ocular stereographic system. The bi-ocular system will eventually be expanded to a binocular system that will provide separate images to both eyes, meeting the final goal of a full-color, variable focus stereographic display.

References

Agilent Technologies (2001) Photograph of MEMS medical diagnostic chip. See web at www.chem.agilent.com/cag/feature/8-98/feature.html.

Ashizaki, K., Yamamoto, M., Miyaoka, S., and Tamada, S. (1994) Apparatus for direct display of an image on the retina of the eye using a scanning laser. *US Patent* #5355181, issued Oct. 11, 1994.

Beachley, N., Harrison, H. (1978) *Introduction to Dynamic System Analysis*. Harper and Row, New York, p. 107 and 130.

Beyer, W. H. (1987) *CRC Standard Mathematical Tables,* 28th ed. CRC Press, Boca Raton, FL, p. 198 and 222-223.

Boff, Kenneth R., and Lincoln, Janet E. (1988) Human Perception and Performance. In *Engineering Data Compendium* (Volume I). Wright-Patterson Air Force Base, Ohio.

Bohringer, Karl F. (2002) *Introduction to Microelectromechanical Systems*, University of Washington EE 502 course notes. See web at www.ee.washington.edu/class/502/aut01/Lectures/ee502-1.pdf.

Burley, G., Stilburn, J., Walker, G. (1998) Membrane mirror and bias electronics. *Applied Optics*, vol. 37(21), p. 4649-4655.

CFAO, Center for Adaptive Optics. An NSF science and technology center. See web at http://cfao.ucolick.org.

Cronos MUMPS MEMS design and fabrication process (2000). See web at www.memsrus.com/cronos/svcsmumps.html.

Denton, D., Diorio, C., and Willows, D. (1999) MEMS probe tips for intercellular neuronal recording. University of Washington Department of Electrical Engineering. See web at www.ee.washington.edu/research/mems/Projects/NeuralProbe.

Depth Cube, Inc. (2001) See web at http://www.3dmedia.com/DepthCube.htm.

Dickensheets, D., Ashcraft, P., Himmer, P. (1999) Pixel-by-pixel aberration correction for scanned-beam micro-optical instruments. *SPIE Conference on Miniaturized Systems with Micro-Optics and MEMS*, September 1999. SPIE vol. 3878, p.48-57.

Dickensheets, D., Himmer, P., Friholm, R., Lutzenberger, B. (2000) Miniature high-resolution imaging system with 3-dimensional MOEMS beam scanning for Mars

exploration. *MOEMS and Miniaturized Systems*, September 2000. SPIE vol. 4178, p. 90-97.

Discera Microcommunications Technologies (2001) See web at www.discera.com/technology.htm.

Ealey, Mark. (1991) Active and Adaptive Optical Components: The Technology and Future Trends. *Active and Adaptive Optical Components.* SPIE vol. 1543, p. 2-13.

Furness, Thomas A. III and Kollin, J. (1995) Virtual Retinal Display. *US Patent* #5467104, issued Nov 14, 1995.

Grace, Roger (2000) The new MEMS and their killer apps. *Sensors Online Magazine*, July 2000. See web at www.rgrace.com/Papers/killerapps.htm.

Grosso, R., Yellin, Y. (1977) The membrane mirror as an adaptive optical element. *The Journal of the Optical Society of America*, March 1977, vol. 67(3), p. 399-406.

Halle, Michael. (1997) Autostereoscopic displays and computer graphics. *Computer Graphics, ACM SIGGRAPH*, vol. 31(2), p. 58-62.

imi-MEMS, Integrated Micro Instruments (2001). Photograph of accelerometer. See web at www.imi-mems.com/ images/zaxis.gif.

Intellite, Inc. (2002) Manufacturer of MEMS deformable membrane mirrors. See web at www.intellite.com/MembraneDMs3_files/frame.htm.

I-O Display Systems (2001) See web at http://www.i-glasses.com/Store/SVGA.php3.

Julesz, B. (1960) *Bell Systems Technical Journal*, vol. 39, p. 1125-1162.

Kaiser Electro-Optics, Inc. (2001) See web at: http://www.keo.com/SIMEYE100A.htm.

Kovacs, Gregory. (1998) *Micromachined Transducers Sourcebook*. WCB McGraw-Hill, Boston, p.31-35.

Langer, Robert (2002) MIT Department of Chemical Engineering. See web at http://web.mit.edu/cheme/research/biological.html

Lucent Technologies (2000) Photograph of MEMS optical switch. See web at www.spie.org/web/oer/august/ aug00/cover1.html.

Mansell, Justin (2002) Deformable Mirror Modeling Software, Version 1.0. See web at http://www.intellite.com/DMModelManual_DMs2.PDF.

Mansell, Justin and Byer, Robert L. (1998) Micromachined Silicon Deformable Mirror. *SPIE Adaptive Optical System Technologies*. SPIE Proceedings, vol. 3353.

Martin, E., Rafael, R., Zapatero-Osorio, M. (1997) The Discovery of Brown Dwarfs. *American Scientist*, Nov.-Dec. 1997. See web at http://www.sigmaxi.org/amsci/articles/97articles/mdiscoveries.html.

Microvision, Inc. (2002) Retinal display systems technology. See web at http://www.mvis.com/tech_disp.htm

Mills, P., Fuchs, F., Pizer, S. (1984) High-speed interaction on a vibrating-mirror 3D display. *Processing and Display of Three-Dimensional Data II*. SPIE vol. 507, p. 93.

Miyao, M., Ishihara, s.Y., Saito, S., Kondo, T.A., Sakakibara, H., and Toyoshima, H. (1996) Visual accommodation and subject performance during a stereographic object task using liquid crystal shutters. *Ergonomics*, vol. 39(11), p. 1294-1309.

Mon-Williams, M., Wann, J., Rushton, S. (1993) Binocular vision in a virtual world: visual deficits following the wearing of a head-mounted display. *Ophthalmic and Physiological Optics*, vol. 13, p. 387-391.

Morse, P.M. (1948) *Vibration and Sound*. 2nd Edition. McGraw-Hill, New York, p. 191-213.

OKO-Tech (2001) Flexible-Optical B.V. Manufacturer of MEMS deformable membrane mirrors. See web at www.okotech.com

Pfeiffer, Eric W. (2001) Micromachines: They're Huge. *Forbes ASAP, A Forbes Supplement.* April 2, 2001, p. 41.

Rinalducci, E. (1983) *Video Displays, Work, and Vision*. National Academy Press, Washington, D.C., p. 143.

Senturia, Stephen (2000) *Microsystem Design*. Kluwer Academic Publishers, Boston, p. 5.

StereoGraphics Corporation (2000) SynthaGram™ Monitor. See web at www.stereographics.com/synthagram/synthagramtechinfo.html

Sugihara, T., Miyasato, T. (1998) A lightweight 3-D HMD with accommodative compensation. *Proceedings of the Society for Information Display 1998*, 32.4. See web at http://www.sid.org/sid98/data/32_04.PDF.

Suyama, S., Date, M., Takada, H. (2000) Three-dimensional display system with dual-frequency liquid-crystal varifocal lens. *Japanese Journal of Applied Physics*, vol. 39, p. 480-484.

Suyama, S. Takada, K. Uehira, S. Sakai, S. Ohtsuka, S. (2001) A New Method for Protruding Apparent 3-D Images in the DFD (Depth-Fused 3-D) Display. *Proceedings of the Society for Information Display 2001*, 53.3, p. 1300-1303.

Texas Instruments (1997) Diagram of Digital Micromirror Device. See web at www.vxm.com/TIDLP.html

Texas Instruments (2002) Digital Light Processing (DLP) technology. See web at www.dlp.com/dlp/default.asp.

Thomas, D.J. (1993) Toward more reliable printed stereo. *Journal of Molecular Graphics and Modeling*, vol. 11(1), p. 15-22.

Tidwell, M. (1995) *A Virtual Retinal Display for Augmenting Ambient Visual Environments*. Thesis (Master). University of Washington College of Electrical Engineering.

Travis, A.R.L. (1997) The Display of Three-Dimensional Video Images. *Proceedings of the IEEE*, vol. 85(11), p. 1817-1832.

Varian Vacuum Products (1992) *Basic Vacuum Practice*, 3rd Edition. Lexington, MA., p. 40.

Vdovin, G. and Sarro, P.M. (1995) Flexible mirror micromachined in silicon. *Applied Optics*, vol. 34, (16), p. 2968-2972.

Voxel, Inc. (2001) Digital holography for a life-size, true 3-D view of medical imagery for surgeons. *Advanced Imaging*, vol. 16, p. 13.

Wann, John P., Rushton, S. Mon-Williams, M. (1995) Natural problems for stereoscopic depth perception in virtual environments. *Vision Research*, vol. 35(19), p. 2731-2736.

Wise, Kensall D. (2001) University of Michigan Department of Electrical Engineering and Computer Science. See web at www.eecs.umich.edu/~wise/Research/Overview/Wise_R.

Appendix A

Deformable membrane mirror instructions as supplied by OKO Tech

Setup:

1. To unpack: open the box removing two corner screws.
2. Very carefully release the mirrors; do not apply any force to the mirror chips.
3. Very carefully remove the protective lids from the mirror membrane chips. This must be done very gently; any mechanical contact with the membrane will destroy the device.

Operation and Handling:

The device is sensitive to static electricity. Keep terminals connected when not in use. Any mechanical contact with the membrane will destroy the mirror. Keep the membrane covered when stored.

To operate the mirror, apply the control DC voltage in the range 0 to 340 V to the mirror terminals. Mounting hole and the mirror chip with membrane must be grounded, control voltage to be applied to the red wire.

Both mirrors were tested interferometrically; the optical power of 2D is achieved with control voltage of 0 to 330 V. Voltage in excess of 340V will destroy the device! Mirror is flat initially with deviation from plane not to exceed 700 nm. Response time- less than 1 ms.

Any device destroyed within 3 days after it is received (Fed Ex tracked delivery) will be replaced for free (buyer pays only Fed Ex s/h). In this case a photograph of the destroyed device should be emailed to gleb@okotech.com immediately.

Appendix B

Voltages for static and dynamic driving of deformable mirror

Static driving

The DMM is fed a positive signal. The gain of the driver is –112, so to drive the mirror statically a negative DC voltage is fed to the driver.:

$$V_{mirror} = -112 * (-\text{DC voltage to driver})$$

Dynamic driving

For dynamic driving, a negative DC voltage is required to shift the AC peak-to-peak voltage down to an all-negative signal, which becomes positive when multiplied by the negative driver gain.

Table B. AC and corresponding DC voltages for dynamic operation of the mirror

AC pp	DC	|Vmirror| (pp)
2.6	-1.3	302
2.4	-1.2	278
2.3	1.15	266
2.2	-1.1	254
2	-1	230
1.8	-0.9	208
1.6	-0.8	186
1.4	-0.7	164
1.2	-0.6	140
1	-0.5	116
0.8	-0.4	92.8
0.6	-0.3	69.6
0.4	-0.2	46.4
0.2	-0.1	23.2
0	0	0

The AC and DC voltages are related by the following equation:

$$DC_{offset} = -1/2\ (AC_{pp})$$

The peak-to-peak output voltage to the mirror is:

$$V_{mirror\ (pp)} = 112 * (AC_{pp} \text{ voltage to driver})$$

Although the output peak-to-peak voltage on the mirror is theoretically 112 times the AC peak-to-peak voltage, there are slight discrepancies between theoretical and actual output voltages because of variations in the driver. Table B shows the AC and DC voltages for dynamic driving of the mirror and the corresponding actual peak-to-peak voltages on the mirror.

Appendix C

Operation of the deformable membrane mirror driver

Power-Up

1. Turn on +5V switch

2. Turn on red O/P control switch

3. Make sure oscilloscope has correct values for the negative DC signal (for static driving) or the AC and corresponding ***negative*** DC current (for dynamic driving).

4. Turn on high-voltage 400 V switch.

To turn off:

1. turn off high-V 400 V switch

2. turn off 5V switch

3. turn off red O/P control switch